



HAL
open science

Examination of ye'elinite formation mechanisms

Y. El Khessaimi, Y. El Hafiane, A. Smith

► **To cite this version:**

Y. El Khessaimi, Y. El Hafiane, A. Smith. Examination of ye'elinite formation mechanisms. Journal of the European Ceramic Society, 2019, 39 (15), pp.5086-5095. 10.1016/j.jeurceramsoc.2019.07.042 . hal-02321714

HAL Id: hal-02321714

<https://unilim.hal.science/hal-02321714>

Submitted on 20 Jul 2022

HAL is a multi-disciplinary open access archive for the deposit and dissemination of scientific research documents, whether they are published or not. The documents may come from teaching and research institutions in France or abroad, or from public or private research centers.

L'archive ouverte pluridisciplinaire **HAL**, est destinée au dépôt et à la diffusion de documents scientifiques de niveau recherche, publiés ou non, émanant des établissements d'enseignement et de recherche français ou étrangers, des laboratoires publics ou privés.



Distributed under a Creative Commons Attribution - NonCommercial 4.0 International License

Examination of ye'elimite formation mechanisms

Y. EL KHESSAIMI, Y. EL HAFIANE, A. SMITH

IRCER, UMR CNRS 7315, Université de Limoges, Centre Européen de la Céramique, 12 avenue Atlantis,
87068 Limoges cedex.

Corresponding author: agnes.smith@unilim.fr

Abstract

Ye'elimite is the main constituent of calcium sulfoaluminate (CSA) cement and one of the major constituents of belite sulfoaluminate or belite sulfoaluminate ferrite cements. The main objective of this work is to describe precisely the formation mechanisms of ye'elimite by solid-state reaction. Mineralogical composition development was monitored using XRD analysis, while microstructural monitoring was conducted using BSE-SEM coupled to EDS analysis. The results show that CaAl_2O_4 and CaAl_2O_7 are the main intermediate products during ye'elimite formation. At the microstructural scale, ye'elimite forms on calcium aluminate phases. Finally, Avrami's model was suggested to discuss the ye'elimite formation rate according to sintering temperature and duration.

Keywords

Ye'elimite; Calcium aluminate; Calcium sulfoaluminate cement; Avrami model; BSE-SEM; EDS mapping.

1. Introduction

Concrete is the most widely used construction material in the world. Ordinary Portland Cement (OPC) has traditionally been used as the binder material in concrete [1]. However, the production of OPC cements contributes of approximately 5% of global anthropogenic CO_2 emissions [2]. The cement industry is making strong effort to reduce the CO_2 footprint in basically three directions: improvement of the fabrication process, development of low CO_2 cements, use of Supplementary Cementitious Materials (SCM) to mix with cement. Belite-CalciumSulfoaluminate-Ferrite cements

(BCSAF) or Calcium SulfoAluminate cements (CSA) are potential alternative cementitious binder for OPC cements [3,4]. The production of calcium sulfoaluminate clinkers involves lower embodied energy and CO₂ emissions compared to the Ordinary Portland Clinker, because they require less limestone, lower grinding energy and lower clinkering temperatures than OPC clinker [5].

Ye'elimite (Ca₄Al₆O₁₆S or C₄A₃ \bar{S})* is a significant component in BCSAF and CSA cements [5]. The detailed understanding of ye'elimite formation during the thermal treatment may be the key for solving burnability[†] encountered during the production of CSA type clinkers. Table 1 shows the cement phases present in CSA clinkers compositions given in the literature [6–12]. It is absolutely clear that on top of ye'elimite CSA clinker products contain various calcium aluminate phases as minor phases. Similar observations were made during pure ye'elimite powder preparation by solid-state reaction methods [6,13–19] or by low temperature chemical routes [20,21], where the final product contained CaO, CaAl₂O₄ and CaAl₄O₇ as main impurities when the sintering temperature was below 1300°C. Hence, successful preparation of highly pure ye'elimite powder by solid-state reactions required multiple milling, pelleting and firing cycles at 1300°C. However, the question of how these successive processing steps increased the ye'elimite content was not raised. Table 2 represents the possible reactions involved during ye'elimite formation in different temperature ranges [19]. Solid-state formation of ye'elimite from pure raw materials starts at 1000°C and it continues until 1300°C through reactions between calcium aluminate phases (CA, CA₂) and CaSO₄ until 1300°C. In this temperature range, CA and CA₂ can be qualified as 'intermediate' compounds since they form between 1000 and 1100°C. From 1300°C, ye'elimite can decompose into calcium aluminate phases (CA and C₁₂A₇), O₂ gas and SO₂ gas. Li et al. [22] studied the formation of ye'elimite from C₃A and gypsum; they reported that the optimal conditions for C₄A₃ \bar{S} formation were 1150 to 1350°C for 1 h to 6 h. Ca²⁺ and SO₄²⁻ were the diffusive species in both the different reactions. Nonetheless, there is no suitable study at microstructural scale involving ye'elimite formation from pure Al₂O₃, CaO and CaSO₄.2H₂O phases.

* The cement phase notations are used in this work (C = CaO, A = Al₂O₃, \bar{S} = SO₃, \bar{C} = CO₂, H = H₂O).

[†] The facility with which the components of CSA cements raw mixture are combined.

As shown by reactions R6 and R7 (table 2), ye'elinite formation involves calcium aluminate phases (CA and CA₂). The microstructural changes happening during the formation of calcium aluminates are well described in literature (which is not the case for ye'elinite). For example, Iftekhar et al. [23] studied the formation of CA from a mixture of CaCO₃-Al₂O₃ powders in a temperature range between 1300 and 1500°C. The authors noted that Ca²⁺ ions diffuse through calcium aluminates and react with alumina, the dense layer of CA₂ formed around the A/CA₂ contact region acts then as a diffusion barrier. The high calcium concentration observed at the pore surface may be an indication that Ca²⁺ diffusion during phase formation occurs at the grain surface. Other authors do not confirm this last hypothesis about the formation of phases in the direction of the interface but confirm the fact that Ca²⁺ diffuse through the calcium aluminates, from calcium-rich aluminates to calcium-poor aluminates [24] [25]. De Bilbao et al. [26] studied the corrosion kinetics of high-alumina refractories by a binary slag (Al₂O₃ 50 wt.% CaO 50 wt.%) at 1650°C for 30 min. It was observed via scanning electron microscopy that CA₆/CA₂ layers formed around the alumina aggregates. The formation of these layers has been explained by the diffusion of Ca²⁺ and O²⁻ ions, and the existence of each layer depends on the temperature. Mercury et al. [27] studied the formation of CA phase from a mixture of Al₂O₃ and CaCO₃ milled by attrition and from a Al(OH)₃ and CaCO₃ powder mix. From 900°C, the formation of mayenite C₁₂A₇ occurs at the contact between the CaO grains and the alumina particles. At higher temperatures, Ca²⁺ ions of calcium-rich phases diffuse through the C₁₂A₇ phase layer to then form the CA phase and so on for the formation of the CA₂ phase. Once these reactions are complete, the densification starts from 1250°C onwards. Scian et al. [28] also studied the formation of the calcium aluminate phase CA, and identified two steps in the process of its formation. During the first stage (short duration and low temperature), the reaction between CaO and Al₂O₃ produces a layer of calcium aluminate at a controlled rate by an interface process (chemical reaction, nucleation and product growth). Then, inside this interface of reaction, separating the two reagents, the calcium (free or combined), diffuses to react with the alumina rich phases and diffusion was identified as the limiting step of the reactions [29].

As far as we learned from the literature [13,16–19,21,30–34], ye’elimite-rich cements present high compressive strength at early age of hydration. Industrial producers of this type of cements seek to obtain a clinker with high ye’elimite amounts. The ideal situation is to convert all the raw materials into ye’elimite during a thermal treatment. However, in most cases, the clinker product contains calcium aluminate phases (CA, CA₂) and small quantities of raw materials (Table 1). The presence of cementitious phases other than ye’elimite in calcium sulfoaluminate cements change the hydration properties (workability, early strength properties, expansion and durability) [10,35–40]. In this context, the phenomenological description of ye’elimite formation could help calcium sulfoaluminate cement producers to improve the burnability of the raw materials during the clinkering process and it could also help academic researchers to synthesize lab-made calcium sulfoaluminate cement for crystallographic characterizations and hydration studies. The purpose of the current work is to investigate the ye’elimite formation mechanisms by solid-state reactions from pure raw materials: calcium carbonate (C \bar{C}), alumina (A) and gypsum (C \bar{S} H₂). This study was conducted using X-ray diffraction and scanning electron microscopy to get information about mineralogical and microstructural assemblages at different synthesis temperatures. Avrami’s model was suggested to highlight the effect of synthesis conditions on ye’elimite kinetic formation.

2. Experiments

2-1- Materials

The starting materials used in this work were high purity CaCO_3 , Al_2O_3 and $\text{CaSO}_4 \cdot 2\text{H}_2\text{O}$ all from Sigma-Aldrich. Table 3 shows the chemical analysis and physical characteristics of these raw materials. The samples were prepared in the form of pellets from stoichiometric mixtures (SM) according to the protocol mentioned in [19]. Each mixture (102 g) was first homogenized in a Turbula[®] shaker for 15 min. Then it was crushed and homogenized again at 120 rpm for 1 h in planetary ball mills, using a 250 ml corundum jar and fifty corundum balls of 10 mm diameter. The homogenized mixture was uniaxially pressed under a load of 1 ton into pellets using a 20 mm cylindrical die. The compacted green body was subsequently placed in a platinum crucible and thermally treated. Table 4 shows the sample identification names and the corresponding thermal cycles (one or two cycles) for each prepared sample. The choice of 1300°C for isothermal study is based on the results of our previous work [19] on pure ye'elimite synthesis since we found that 1300°C was the optimal ye'elimite synthesis temperature. The heat treatment from 1100 to 1300°C were performed in a platinum crucible and in an elevator-furnace to ensure air quenching. To avoid the degradation of the elevator-furnace heating elements, experiments at 1000°C were carried out in muffle furnace without air quenching.

2-2- Characterization techniques

The scanning electron microscope (SEM, JSM-IT300, JEOL, Japan) used for this study was equipped with an Energy Dispersive Spectrometer (EDS, Oxford, UK). The microscope was operated at 15 kV accelerating voltage. Prior to any observation, a 15 nm Au-Pd or Carbone coating was deposited in order to ensure suitable electronic conduction at the surface of samples. The specimens were stored in desiccators filled with silica gel prior to and after examinations to prevent hydration or carbonation. Colored Backscattered Electron (BSE) images reveal the different phases because of the atomic number contrast. EDS mapping and compositional profile along a line were made to localize each formed phase. For reliable observations, the essential prerequisite is a well-polished sample. Polished sections can provide representative images of a cross section of the

samples microstructure. In this respect, the impregnation of the sample (under the form of a pellet) is done with a low-viscosity epoxy resin (IP, PRESI France). The hardening time of the resin is about 24 h at room temperature. Once the sample is removed from the mold, the top side of the embedded sample is polished using SiC paper and absolute ethanol as a lubricant. Water should not be used at any time as it could lead to hydration of anhydrous grains. Regular observation of the surface under a light microscope is essential to check the surface aspect after each polishing step. Polishing was performed using Minitech 233 type machine (Presi, France). Details of the polishing protocol are given in table 5.

X-Ray Diffraction (XRD) data were collected at room temperature in the Bragg-Brentano geometry using a Bruker D8 Advance X-ray diffractometer with $\text{CuK}\alpha$ radiation ($\lambda_{\text{Cu}} = 1.54056 \text{ \AA}$, without monochromator) at a step scan of 0.02° with a time counting per step of 0.45 second operated at a voltage 40 kV and an electric current 40 mA. The sample was rotated during data collection at 15 rpm in order to increase particle statistics. The diffractometer was equipped with energy-dispersive LYNXEYE XE-T detector for filtration of fluorescence and $\text{K}\beta$ radiation. Table 6 shows ICSD (Inorganic Crystal Structure Database) collection codes used for XRD phase identification [34,41–44].

The particle size distribution (PSD) of the raw powders was obtained using a Mastersizer 2000 laser size analyzer (Malvern). Prior to this measurement, the powder (approximately 80 mg) was mixed in 20 ml of absolute ethanol and the suspension was sonicated 1 min in order to break the coarse agglomerates. The BET specific surface area was estimated from N_2 adsorption experiments using a Micromeritics model Tristar®II 3020 analyzer. Prior to measurements, a degassing step of the sample powder was carried out at 80°C overnight in order to achieve a pressure equal to 60 mTorr.

Chemical analyses of the raw materials powders were carried out using X-ray fluorescence spectrometer, PANalytical, Zetium model. Samples were prepared as fused beads using glass discs prepared by melting about $1 \pm 0.001 \text{ g}$ of sample powder with $10 \pm 0.001 \text{ g}$ of lithium tetra borate flux. The Loss on Ignition (LOI) was calculated for samples treated at 1050°C for 1 h. The oxide contents are expressed in weight percent (wt.%).

3. Results and discussion

3-1- Mineralogical analysis

Fig. 1 represents X-Ray diffractograms of the samples heated between 1000 to 1300°C for 3 h. For temperatures ranging from 1000 to 1200°C, the diffraction peaks with the main intensities correspond to CaO (C), Al₂O₃ (A) and CaSO₄ (CS̄). The peaks for ye'elimite (C₄A₃S̄) and krotite (CA) are much smaller. The appearance of CaSO₄ and CaO phases is attributed to the decomposition of gypsum and CaCO₃, respectively (reactions R1 and R2 in table 2). At 1100°C, CA₂ diffraction peaks appear, while those related to CaO and Al₂O₃ are attenuated. Grossite (CA₂) forms by the solid-state reaction between CaO and Al₂O₃ (reaction R5 in table 2) [27]. From 1100 to 1200°C, the diffraction intensities of CaO and Al₂O₃ are attenuated while those of CA and CA₂ peaks are slightly more intense; this variations in peak intensities can be related to the crystallisation of calcium aluminates (reactions R3 and R5, Table 2) [27]. Beyond 1200°C, the peak intensities of CA and CA₂ decrease while the peak intensities of ye'elimite increase; this last phase can form through solid-state reaction between calcium aluminates and calcium sulphate reactions R6 and R7 (table 2) [19]. Hence, the reaction of ye'elimite formation is well activated by increasing sintering temperature, especially from 1200 to 1300°C.

Fig. 2 shows the XRD patterns of the samples heated at 1300°C for various durations, from 15 to 180 min. CaO, CaSO₄, Al₂O₃, CA, CA₂ and ye'elimite were identified in the sample heated at 1300°C and immediately quenched (dwell time at 1300°C : 0 min). By increasing the dwell time from 0 to 180 min, CA diffraction peaks become more intense, while those related to CaO, Al₂O₃ and CaSO₄ are attenuated. Simultaneously, the intensity of the peaks related to ye'elimite phase increases with increasing the dwell time with a simultaneous decrease in calcium aluminate peak intensities. This confirms the conversion of calcium aluminate phases to ye'elimite phase according to the reactions R6 and R7 (table 2). Hence, the reaction of ye'elimite formation is well activated by increasing the dwell time at 1300°C.

The XRD results can be summarized as follows: (i) ye'elimite starts forming at 1000°C; (ii) CA and CA₂ are intermediate phase formed between 1000 and 1100°C; (iii) above 1100°C, CA (resp. CA₂) progressively react with C \bar{S} through R6 (table 2), (resp. C and C \bar{S} through R7, table 2) to convert into ye'elimite.

3-2- Microstructural observation

The observed microstructural changes during ye'elimite formation are shown in fig. 3 and fig. 4. The colored EDS mapping of back-scattered electron images for the samples sintered at different temperatures (from 1000 to 1300°C) for 3 hours are shown in fig. 3. The following descriptions can be made: samples treated at 1000°C present a heterogeneous microstructure with the presence of three materials, namely Al₂O₃, CaO and CaSO₄. CaO and CaSO₄ come respectively from CaCO₃ decarbonation and CaSO₄.2H₂O dehydration. After sintering at 1100°C, small amounts of CA and CA₂ are formed around fine alumina grains. Similar observations can be made for the sample sintered at 1200°C. By increasing the temperature to 1250°C, the CA layer around alumina aggregates thickens while alumina grains decrease in size. We also see C₄A₃ \bar{S} grains formed thanks to the reaction between CA and CaSO₄ grains. As the temperature increases to 1300°C, the CA phase almost totally surrounds alumina grains whose size reduces considerably. These observations are in accordance with the XRD results shown in fig. 1.

After the examination of the microstructural changes as a function of heating temperature, it is interesting to look at the microstructural changes as a function of dwell time for a given temperature. Colored EDS mapping of back-scattered electron images for the samples sintered at 1300°C from 15 to 180 min are shown in Fig. 5. After 15 min heat treatment at 1300°C, ye'elimite surrounds CA and CA itself surrounds Al₂O₃ grains (fig. 4a). Some lime grains are present. For the sample sintered for 30 min, we notice the presence of a core of Al₂O₃ grains surrounded by CA₂, CA and an external layer of C₄A₃ \bar{S} (fig. 4b). For the sample sintered for longer time (60 and 120 min, fig. 4c and 4d), C₄A₃ \bar{S} becomes dominant compared to CA and Al₂O₃. Lastly, after 180 min, large C₄A₃ \bar{S} grains are

formed and no Al_2O_3 , CaO and CaSO_4 are left (fig. 4e). It clearly shows that the formation of ye'elimite is almost complete for sintering duration above 120 min.

Fig. 5a corresponds to EDS data of atomic percentage for calcium, aluminum and sulfur elements as a function of the position on the scan line for the sample heated at $1300\text{ }^\circ\text{C}$ for 30 min (see the red line on fig. 4b). We can obviously identify four zones in fig. 5a. To identify the compositions corresponding to each zone, the data are plotted in atomic percentage in the ternary composition diagram Al-Ca-S (fig. 5b). Four regions can be distinguished: the first is Al_2O_3 rich (blue ellipse), the second is close to CA_2 (red ellipse), the third is close to CA (green ellipse) and the last one is close to $\text{C}_4\text{A}_3\bar{\text{S}}$ (pink ellipse). Thus, CA_2 phase tends to form on Al_2O_3 grains, then CA phase tends to form on CA_2 grains and $\text{C}_4\text{A}_3\bar{\text{S}}$ forms on CA grains according to solid-state reaction R5 (table 2).

3-3- Discussion

Based on the XRD analysis and the microstructural observations, ye'elimite amount increases as the sintering temperature goes from 1000 to $1300\text{ }^\circ\text{C}$ for 3 h. However, it is still not pure at $1300\text{ }^\circ\text{C}$ since some CA, CA_2 , CaO , Al_2O_3 and CaSO_4 remain. The presence of these phases could be explained by an incomplete solid-state reaction between the different reactants.

Fig. 6a summarizes the possible solid-state diffusion during ye'elimite formation. Fig. 6b and 6c give a schematic representation of the microstructure transformations as a function of temperature for a given duration (fig. 6b) and as a function of dwell time at $1300\text{ }^\circ\text{C}$ (fig. 6c). Based on the literature [22], we assume that the diffusive species are Ca^{2+} and SO_4^{2-} . Ca^{2+} ions coming from CaO can reach the CA/ CA_2 interface and react with CA_2 to produce CA (reaction (a), fig. 6a); the consequence is a growth of CA grain and a consumption of CA_2 (the movement of the CA/ CA_2 interface is schematized by arrow 1, fig. 6a). Alternatively, CA can decompose into CaO – thus producing Ca^{2+} ions – and CA_2 (reaction (b), fig. 6a); the result is a growth of CA_2 grain and a decrease of CA (the displacement of the CA/ CA_2 interface is schematized by arrow 2, fig. 6a). The Ca^{2+} ions can also reach the next interface $\text{CA}_2/\text{Al}_2\text{O}_3$ and consume alumina to form CA_2 (reaction (c) with a growth of CA_2 and a decrease in size of Al_2O_3 , arrow 3). For the outer layer which contains $\text{C}_4\text{A}_3\bar{\text{S}}$ phase, its

growth depends upon the contact between CA phase and CaSO₄ phase. Ca²⁺ and S^{VI+} may diffuse from CaSO₄ grains to C₄A₃ \bar{S} /CA and/or to C₄A₃ \bar{S} /CA₂ to form C₄A₃ \bar{S} (reactions R6 and R7, table 2). Fig. 6b and fig. 6c give a schematic representation of the microstructural evolutions. As the temperature increases (fig. 6b), the Al₂O₃ grains progressively disappear and are replaced by CA and CA₂. These two compounds themselves eventually transform into ye'elimite. From microstructural observations of samples treated at 1300°C for different durations (fig. 4), the schematic representation on fig. 6c represents what happens: Al₂O₃ grains then calcium aluminate phases present at 1300°C are progressively consumed to give C₄A₃ \bar{S} -rich regions.

Avrami's kinetic model based on geometrical contraction of reactant grains, can be qualitatively applied to our case. ~~Quantitative calculations cannot be done because the grains geometry is more complex than simple spheres. Nevertheless,~~ Avrami's This model enables us to identify the parameters which influence upon the microstructural changes as a function of time or temperature. The rate of a solid-state reaction is described by equation (4) [45]:

$$\frac{d\sigma}{dt} = k f(\sigma) \quad \text{Eq.(4)}$$

where σ is the conversion fraction given by equation (5), $f(\sigma)$ is the function of the reaction model and k is the reaction rate constant, k is usually given by the Arrhenius equation (equation 6) [46]:

$$\sigma = \frac{m_0 - m_t}{m_0 - m_\infty} \quad \text{Eq.(5)}$$

m_0 is the initial reactant weight, m_t is the reactant weight at sintering time t , and m_∞ is the final weight which is generally approximated to be equal to 0 (complete reaction).

$$k = A \cdot e^{-E_a/RT} \quad \text{Eq.(6)}$$

A is the frequency factor, R is the gas constant, T is the sintering temperature and E_a is the activation energy. In the terminology of homogeneous kinetics, the activation energy (E_a) is usually identified as the energy barrier that must be overcome to enable the occurrence of the bond redistribution steps required to convert reactants into products. The pre-exponential term, or frequency factor (A), gives

an indication of the frequency of occurrence of the reaction situation. It is usually dependent upon the vibration frequency of the reaction co-ordinate [47].

Fig. 7 is a schematic representation of the successive layers formed on the surface of Al₂O₃ grain. In the present case, the rate of Al₂O₃ grain consumption is supposed to be controlled by the progress of the interface reaction towards the middle of the grain. The radius (r) at sintering time t is given by equation (7) [45]:

$$r = r_0 - kt \quad \text{Eq.(7)}$$

where r₀ is the radius at time t₀ and t is the solid-state reaction time.

If we make a simple assumption that Al₂O₃ grains are spherical with a volume of $\frac{4\pi r^3}{3}$ and a density ρ , equation (5) becomes:

$$\sigma = \frac{\frac{4}{3}\pi\rho r_0^3 - \frac{4}{3}\pi\rho r^3}{\frac{4}{3}\pi\rho r_0^3} \quad \text{Eq.(8)}$$

which reduces to equation (9):

$$1 - \sigma = \frac{r^3}{r_0^3} \quad \text{Eq.(9)}$$

By combining equation (7) with equation (9) we have:

$$1 - (1 - \sigma)^{1/3} = \frac{k}{r_0} t = f(\sigma) \quad \text{Eq.(10)}$$

By combining equation (4) with equation (6) and (10) we can write:

$$\frac{d\sigma}{dt} = A \cdot e^{(-\frac{E_a}{RT})} \frac{t}{r_0} \quad \text{Eq.(11)}$$

The suggested model expressed by equation (11) highlights qualitatively the effect of the synthesis conditions on ye'elinite formation using a simple 3D-geometrical contraction model. To go further, i.e. to obtain quantitative values for E_a and A, it would be in principle feasible, but their values would be meaningless and would not describe precisely the complex solid-state formation of

ye'elimite. In fact, there are many limitations to discuss quantitatively the application of the proposed model. First, the starting point of theoretical explanation of Arrhenius behavior in homogeneous reactions is the Maxwell-Boltzmann energy distribution function, although this model is inapplicable to immobilized constituents of a solid [47]. Furthermore, the formation process of ye'elimite involves many reactions that occur sometimes simultaneously. Thirdly, the suggested model assumes one value of alumina particle radii. In reality, there is a distribution of alumina particle size and the particles sometimes agglomerate. Since no realistic alternative is capable of expressing the formation rate versus temperature during complex solid-state reactions [47], Avrami's model based on the Arrhenius equation has been widely accepted and successfully applied by many authors to describe numerous reactions involving solids.

In the present case, the proposed sequence is the following: Al_2O_3 converts into CA_2 which in turn transforms into CA. Then CA reacts with CaSO_4 to form $\text{C}_4\text{A}_3\bar{\text{S}}$. So ye'elimite formation depends on Al_2O_3 consumption. Referring to Avrami's kinetic model mathematically expressed by equation (11), Al_2O_3 conversion rate increases with increasing sintering temperature (T), increasing sintering time (t) and/or reducing the size of the starting Al_2O_3 grain (r_0). This could explain qualitatively the high thickness of $\text{C}_4\text{A}_3\bar{\text{S}}$ -rich and CA-rich regions around the smallest Al_2O_3 grains. It should be noted that there is some extreme values for T and t that should not be exceeded due to the sulfate instability above 1300°C as synthesis temperature and/or 4 h duration [19].

4. Conclusion

The reaction sequence by which ye'elimite forms through solid-state reactions from pure raw materials (alumina, lime and gypsum) was studied. First, mineralogical development during ye'elimite formation from 1000 to 1300°C for 3 hours and from 15 to 180 min at 1300°C , shows that ye'elimite content increases with increasing sintering temperature and duration. These results were confirmed by microstructural observations using colored EDS mapping of BSE micrographs. The formation of thick ye'elimite region and the remanence of small alumina grains is explained

qualitatively by the dependence of diffusion rate with sintering temperature, sintering duration and Al_2O_3 grains size. The microstructure forms in different layers going from Al_2O_3 -rich region to $\text{C}_4\text{A}_3\bar{\text{S}}$ -rich region, where Ca^{2+} diffuses from CaO to Al_2O_3 through CA and CA_2 , and $\text{S}^{\text{VI}+}$ diffuse through $\text{C}_4\text{A}_3\bar{\text{S}}$ to calcium aluminate phases to form ye'elimite. It was concluded that CA and CA_2 are the main intermediate products during ye'elimite formation. Finally, the formation rate of ye'elimite could be simply described by the geometrical contracted Avrami's model. This model provides an insight about the relation between alumina consumption grains during clinking and ye'elimite formation.

The results reported herein deepen the understanding of the phenomenological description of ye'elimite solid-state formation, which could help cement producers to improve the burnability of raw materials during the clinkering process of calcium sulfoaluminate cements (ye'elimite-rich cements) and to minimize the presence of secondary phases like calcium aluminate phases. Lastly, the present study could also help academic researchers to synthesize lab-made calcium sulfoaluminate cements for crystallographic characterizations and hydration studies.

References

- [1] H.F. Taylor, *Cement chemistry*, Thomas Telford, 1997.
- [2] C.A. Hendriks, E. Worrell, D. De Jager, K. Blok, P. Riemer, Emission reduction of greenhouse gases from the cement industry, in: *Proc. Fourth Int. Conf. Greenh. Gas Control Technol.*, Interlaken, Austria, IEA GHG R&D Programme, (1998) 939–944.
- [3] T. Hanein, I. Galan, A. Elhoweris, S. Khare, S. Skalamprinos, G. Jen, M. Whittaker, M.S. Imbabi, F.P. Glasser, M.N. Bannerman, Production of belite calcium sulfoaluminate cement using sulfur as a fuel and as a source of clinker sulfur trioxide: pilot kiln trial, *Adv. Cem. Res.* 28 [10] (2016) 643–653. doi: 10.1680/jadcr.16.00018.
- [4] K. Quillin, Performance of belite–sulfoaluminate cements, *Cem. Concr. Res.* 31 (2001) 1341–1349. doi: 10.1016/S0008-8846(01)00543-9.
- [5] E. Gartner, T. Sui, Alternative cement clinkers, *Cem. Concr. Res.* (2017). doi:10.1016/j.cemconres.2017.02.002.
- [6] F. Winnefeld, B. Lothenbach, Hydration of calcium sulfoaluminate cements—experimental findings and thermodynamic modelling, *Cem. Concr. Res.* 40 (2010) 1239–1247. doi: 10.1016/j.cemconres.2009.08.014.
- [7] A. Telesca, M. Marroccoli, M.L. Pace, M. Tomasulo, G.L. Valenti, P.J.M. Monteiro, A hydration study of various calcium sulfoaluminate cements, *Cem. Concr. Compos.* 53 (2014) 224–232. doi:10.1016/j.cemconcomp.2014.07.002.
- [8] L. Pelletier-Chaignat, F. Winnefeld, B. Lothenbach, C.J. Müller, Beneficial use of limestone filler with calcium sulfoaluminate cement, *Constr. Build. Mater.* 26 (2012) 619–627. doi: 10.1016/j.conbuildmat.2011.06.065

- [9] L.H. Martin, F. Winnefeld, C.J. Müller, B. Lothenbach, Contribution of limestone to the hydration of calcium sulfoaluminate cement, *Cem. Concr. Compos.* 62 (2015) 204–211. doi: 10.1016/j.cemconcomp.2015.07.005.
- [10] J. Bizzozero, C. Gosselin, K.L. Scrivener, Expansion mechanisms in calcium aluminate and sulfoaluminate systems with calcium sulfate, *Cem. Concr. Res.* 56 (2014) 190–202. doi: 10.1016/j.cemconres.2013.11.011.
- [11] Q. Zhou, N.B. Milestone, M. Hayes, An alternative to Portland cement for waste encapsulation—the calcium sulfoaluminate cement system, *J. Hazard. Mater.* 136 (2006) 120–129. doi: 10.1016/j.jhazmat.2005.11.038.
- [12] L. Pelletier, F. Winnefeld, B. Lothenbach, The ternary system Portland cement–calcium sulfoaluminate clinker–anhydrite: hydration mechanism and mortar properties, *Cem. Concr. Compos.* 32 (2010) 497–507. doi: 10.1016/j.cemconcomp.2010.03.010.
- [13] F. Winnefeld, S. Barlag, Calorimetric and thermogravimetric study on the influence of calcium sulfate on the hydration of ye’elimite, *J. Therm. Anal. Calorim.* 101 (2009) 949–957. doi: 10.1007/s10973-009-0582-6.
- [14] N. Chitvoranund, B. Lothenbach, F. Winnefeld, J. Skibsted, K. Scrivener, Comparison of different preparation methods for ye’elimite clinker synthesis, Conference: International Workshop on Calcium sulfoaluminate cements At: Murten, Switzerland. (2018) 22.
- [15] C.W. Hargis, A.P. Kirchheim, P.J. Monteiro, E.M. Gartner, Early age hydration of calcium sulfoaluminate (synthetic ye’elimite, $C_4A_3\bar{S}$) in the presence of gypsum and varying amounts of calcium hydroxide, *Cem. Concr. Res.* 48 (2013) 105–115.
- [16] A. Cuesta, A.G. De la Torre, E.R. Losilla, V.K. Peterson, P. Rejmak, A. Ayuela, C. Frontera, M.A. Aranda, Structure, atomistic simulations, and phase transition of stoichiometric yeelimite, *Chem. Mater.* 25 (2013) 1680–1687. doi: 10.1021/cm400129z.
- [17] A. Cuesta, A.G. De la Torre, E.R. Losilla, I. Santacruz, M.A. Aranda, Pseudocubic crystal structure and phase transition in doped ye’elimite, *Cryst. Growth Des.* 14 (2014) 5158–5163. doi: 10.1021/cg501290q.
- [18] G. Álvarez-Pinazo, A. Cuesta, M. García-Maté, I. Santacruz, E.R. Losilla, A.G. De la Torre, L. León-Reina, M.A. Aranda, Rietveld quantitative phase analysis of Yeelimite-containing cements, *Cem. Concr. Res.* 42 (2012) 960–971. doi: 10.1016/j.cemconres.2012.03.018.
- [19] Y. El Khessaimi, Y. El Hafiane, A. Smith, R. Trauchessec, C. Diliberto, A. Lecomte, Solid-state synthesis of pure ye’elimite, *J. Eur. Ceram. Soc.* 38 [9] (2018) 3401–3411. doi:10.1016/j.jeurceramsoc.2018.03.018.
- [20] Y. El Khessaimi, Y. El Hafiane, A. Smith, Ye’elimite synthesis by chemical routes, *J. Eur. Ceram. Soc.* 39 [4] (2019) 1683–1695. doi:10.1016/j.jeurceramsoc.2018.10.025.
- [21] J.-T. Song, J.F. Young, Direct synthesis and hydration of calcium aluminosulfate ($Ca_4Al_6O_{16}S$), *J. Am. Ceram. Soc.* 85 (2002) 535–539. doi: 10.1111/j.1151-2916.2002.tb00129.x.
- [22] X. Li, Y. Zhang, X. Shen, Q. Wang, Z. Pan, Kinetics of calcium sulfoaluminate formation from tricalcium aluminate, calcium sulfate and calcium oxide, *Cem. Concr. Res.* 55 (2014) 79–87. doi: 10.1016/j.cemconres.2013.10.006.
- [23] S. Iftexhar, J. Grins, G. Svensson, J. Lööf, T. Jarmar, G.A. Botton, C.M. Andrei, H. Engqvist, Phase formation of $CaAl_2O_4$ from $CaCO_3$ – Al_2O_3 powder mixtures, *J. Eur. Ceram. Soc.* 28 (2008) 747–756. doi: 10.1016/j.jeurceramsoc.2007.08.012.
- [24] A.N. Scian, J.P. Lopez, E. Pereira, High alumina cements. Study of CaO – Al_2O_3 formation. I. Stoichiometric mechanism, *Cem. Concr. Res.* 17 (1987) 198–204. doi: 10.1016/0008-8846(87)90102-5.
- [25] B. Viswanath, N. Ravishankar, Interfacial reactions in hydroxyapatite/alumina nanocomposites, *Scr. Mater.* 55 (2006) 863–866. doi: 10.1016/j.scriptamat.2006.07.049.
- [26] E. de Bilbao, M. Dombrowski, H. Pilliere, J. Poirier, Time-resolved high-temperature X-ray diffraction for studying the kinetics of corrosion of high-alumina refractory by molten oxides, *Corros. Sci.* 139 (2018) 346–354. doi:10.1016/j.corsci.2018.05.003.
- [27] J.R. Mercury, A.H. De Aza, P. Pena, Synthesis of $CaAl_2O_4$ from powders: Particle size effect, *J. Eur. Ceram. Soc.* 25 (2005) 3269–3279. doi: 10.1016/j.jeurceramsoc.2004.06.021.

- [28] A.N. Scian, J.P. López, E. Pereira, High alumina cements. Study of $\text{CaO} \cdot \text{Al}_2\text{O}_3$ formation II. Kinetics, *Cem. Concr. Res.* 17 (1987) 525–531. doi: 10.1016/0008-8846(87)90124-4.
- [29] B.M. Mohamed, J.H. Sharp, Kinetics and mechanism of formation of tricalcium aluminate, $\text{Ca}_3\text{Al}_2\text{O}_6$, *Thermochim. Acta.* 388 (2002) 105–114. doi: 10.1016/S0040-6031(02)00035-7.
- [30] A. Rungchet, P. Chindapasirt, S. Wansom, K. Pimraksa, Hydrothermal synthesis of calcium sulfoaluminate–belite cement from industrial waste materials, *J. Clean. Prod.* 115 (2016) 273–283. doi: 10.1016/j.jclepro.2015.12.068.
- [31] N. Chitvoranund, F. Winnefeld, C.W. Hargis, B. Lothenbach, Synthesis and hydration of alite-calcium sulfoaluminate cement, *Adv Cem Res.* 29 (2017) 101–111. doi: 10.1680/jadcr.16.00071.
- [32] P.E. Halstead, A.E. Moore, The composition and crystallography of an anhydrous calcium aluminosulphate occurring in expanding cement, *J. Appl. Chem.* 12 (1962) 413–417. doi: 10.1002/jctb.5010120906.
- [33] K. Ikeda, K. Kishimoto, H. Shima, Structure refinement of calcium sulfoaluminate, $\text{C}_4\text{A}_3\bar{\text{S}}$ with emphasis to oxygen deficiency, *Cem. Concr. Res.* 26 (1996) 743–748. doi: 10.1016/S0008-8846(96)85011-3.
- [34] N.J. Calos, C.H.L. Kennard, A.K. Whittaker, R.L. Davis, Structure of calcium aluminate sulfate $\text{Ca}_4\text{Al}_6\text{O}_{16}\text{S}$, *J. Solid State Chem.* 119 (1995) 1–7. doi:10.1016/0022-4596(95)80002-7.
- [35] C.W. Hargis, A. Telesca, P.J.M. Monteiro, Calcium sulfoaluminate (Ye’elimite) hydration in the presence of gypsum, calcite, and vaterite, *Cem. Concr. Res.* 65 (2014) 15–20. doi:10.1016/j.cemconres.2014.07.004.
- [36] F. Bullerjahn, M. Zajac, M. Ben Haha, CSA raw mix design: effect on clinker formation and reactivity, *Mater. Struct.* 48 (2015) 3895–3911. doi:10.1617/s11527-014-0451-z.
- [37] F. Bullerjahn, D. Schmitt, M. Ben Haha, Effect of raw mix design and of clinkering process on the formation and mineralogical composition of (ternesite) belite calcium sulphoaluminate ferrite clinker, *Cem. Concr. Res.* 59 (2014) 87–95. doi:10.1016/j.cemconres.2014.02.004.
- [38] M. Palou, J. Majling, Effects of sulphate, calcium and aluminum ions upon the hydration of sulphoaluminate belite cement, *J. Therm. Anal. Calorim.* 46 (1996) 549–556. doi: 10.1007/BF02135034.
- [39] J.-P. Boisvert, M. Domenech, A. Foissy, J. Persello, J.-C. Mutin, Hydration of calcium sulfate hemihydrate ($\text{CaSO}_4 \cdot 1/2\text{H}_2\text{O}$) into gypsum ($\text{CaSO}_4 \cdot 2\text{H}_2\text{O}$). The influence of the sodium poly (acrylate)/surface interaction and molecular weight, *J. Cryst. Growth.* 220 (2000) 579–591. doi: 10.1016/S0022-0248(00)00865-4.
- [40] M.P. Adams, J.H. Ideker, Volume Stability of Calcium Aluminate Cement and Calcium Sulfoaluminate Cement Systems, *Factors Influ. Convers. Vol. Stab. Calcium Aluminate Cem. Syst.* (2014) 159.
- [41] W. Hörkner, Hk. Müller-Buschbaum, Zur kristallstruktur von CaAl_2O_4 , *J. Inorg. Nucl. Chem.* 38 (1976) 983–984. doi:10.1016/0022-1902(76)80011-5.
- [42] V.I. Ponomarev, D.M. Kheiker, N.V. Belov, Crystal structure of calcium dialuminate, CA_2 , *Sov. Phys. Crystallogr. USSR.* 15 (1971) 995–+.
- [43] D. Grier, G. McCarthy, North Dakota State University, Fargo, North Dakota, USA, ICDD Grant-in-Aid 1991, *Powder Diffr. File Int. Cent. Diffr. Data.* (1994).
- [44] G.C.H. Cheng, J. Zussman, The crystal structure of anhydrite (CaSO_4), *Acta Crystallogr.* 16 (1963) 767–769. doi: 10.1107/S0365110X63001997.
- [45] A. Khawam, D.R. Flanagan, Solid-state kinetic models: basics and mathematical fundamentals, *J. Phys. Chem. B.* 110 (2006) 17315–17328. doi: 10.1021/jp062746a.
- [46] W.D. Kingery, H.K. Bowen, D.R. Uhlmann, Introduction to ceramics, Wiley New York, (1976) 381–447.
- [47] A.K. Galwey, M.E. Brown, Application of the Arrhenius equation to solid state kinetics: can this be justified? *Thermochimica Acta*, 386(1) (2002) 91–98. doi-org.inc.bib.cnrs.fr/10.1016/S0040-6031(01)00769-9

Figure captions

Figure 1	X-Ray diffractograms of samples treated from 1000 to 1300°C for 3 h.
Figure 2	X-Ray diffractograms of samples treated at 1300 °C from 0 to 180 min.
Figure 3	EDS mapping of elements present in the samples treated for 3 h between 1000°C (a), 1100°C (b), 1200°C (c), 1250°C (d) and 1300°C (e). Magnification of x150 was used of all images (Bars represent 250 μm). The corresponding EDS point analysis are shown in Appendix A.
Figure 4	EDS mapping of elements present in the samples treated at 1300°C for different durations: 15 min (a), 30 min (b), 60 min (c), 120 min (d) and 180 min (e). Magnification of x500 was used of all images (Bars represent 50 μm). The red line of the sample treated at 30 min (Fig. 3(a)) represents EDS line-scan, the results of the line scan are shown in Fig. 4 and the corresponding EDS point analyses are shown in Appendix A.
Figure 5	(a) Composition profile obtained by EDS along the red line for the sample treated at 1300°C for 30 min (The EDS line-scan is represented by the red line in Fig. 3), (b) Representation of EDS line scan data in ternary atomic percentage diagram of Al-Ca-S (the red square, represents theoretical atomic composition of CA ₂ , the green square represents theoretical atomic composition of CA and the purple square represents theoretical atomic composition of C ₄ A ₃ S̄. The black triangles are associated to the collected EDS data.
Figure 6	(a) Schematic representation of solid-state diffusion during ye'elimite formation. (b) Schematic representation of microstructural development of ye'elimite formation according to the sintering temperature. (c) Schematic representation of microstructural development of ye'elimite formation according to the sintering duration.
Figure 7	Simple schematic model of reaction-product layers forming on alumina grain.
Appendix A	Typical EDS spectra of samples shown in fig. 3 and fig. 4.

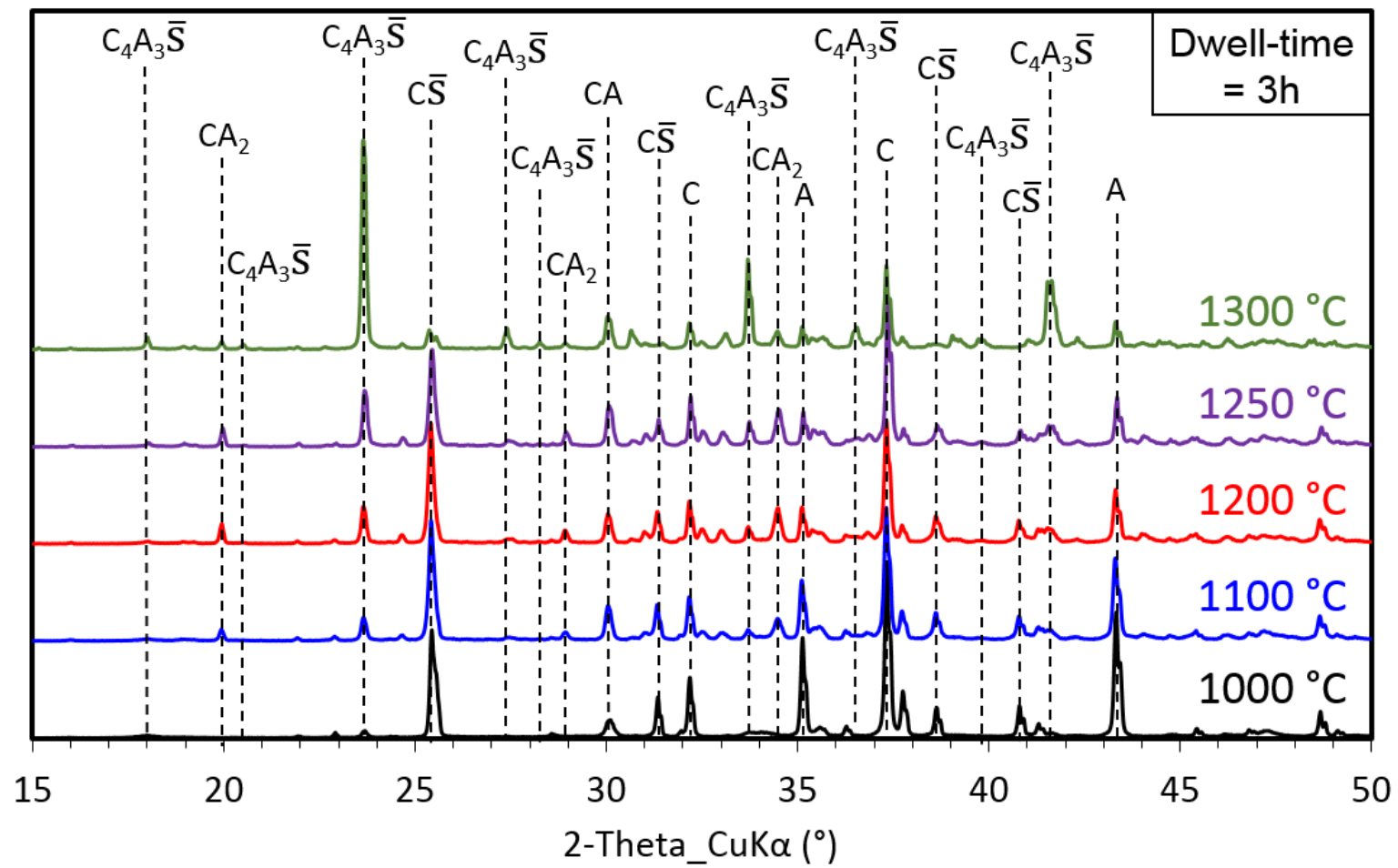


Figure. 1

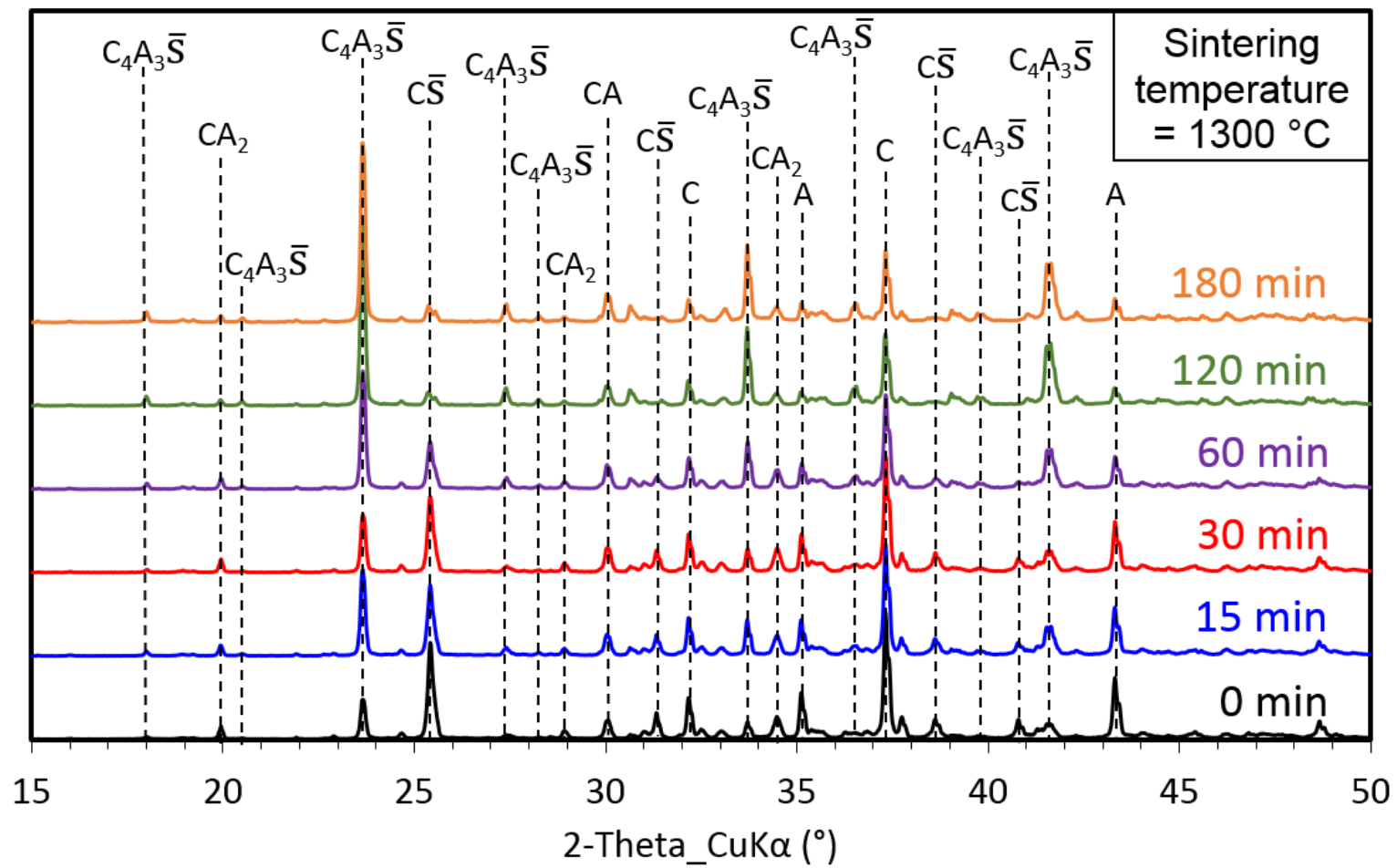


Figure. 2

EDS mapping of BSE images (x150)

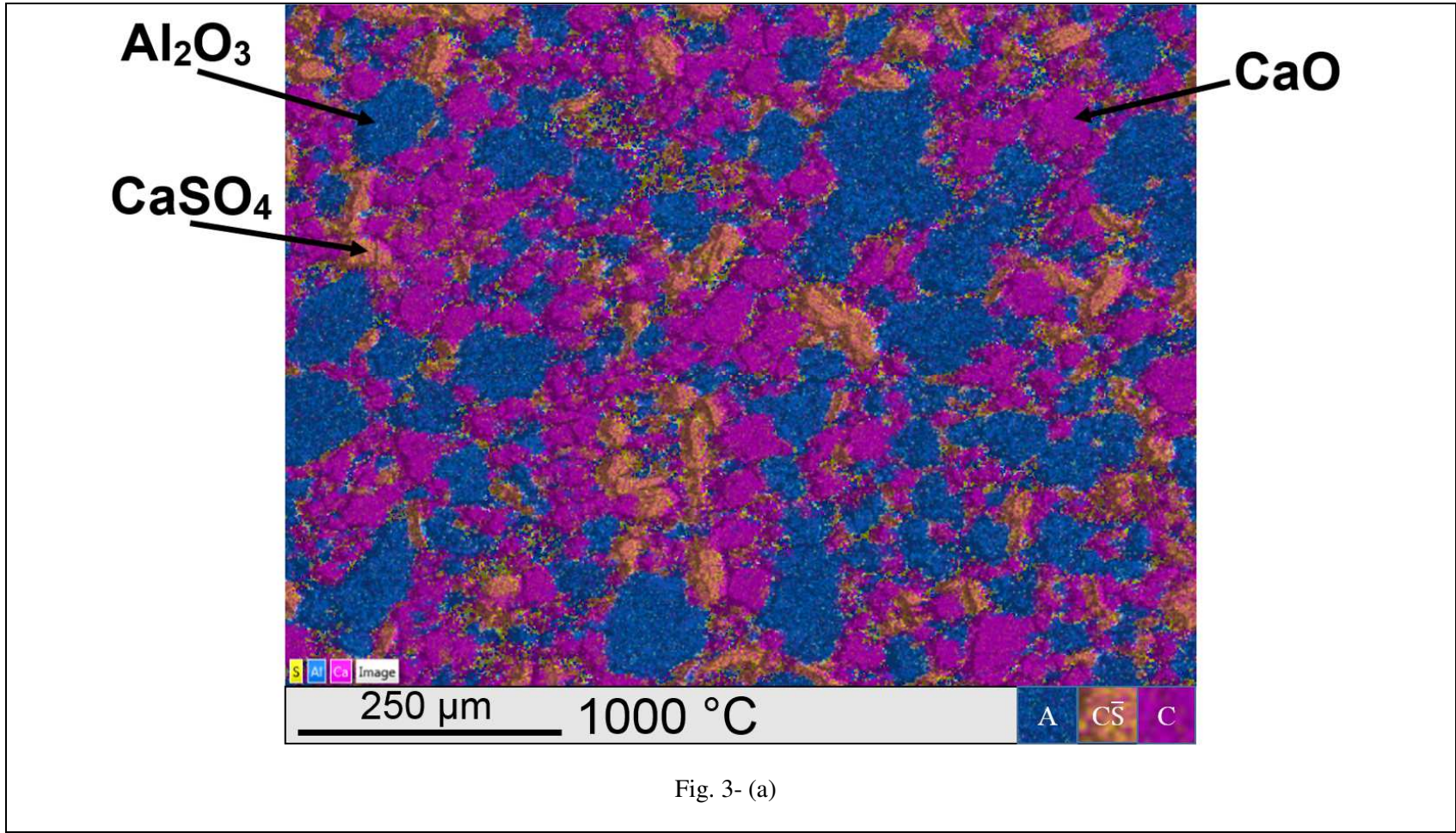


Fig. 3- (a)

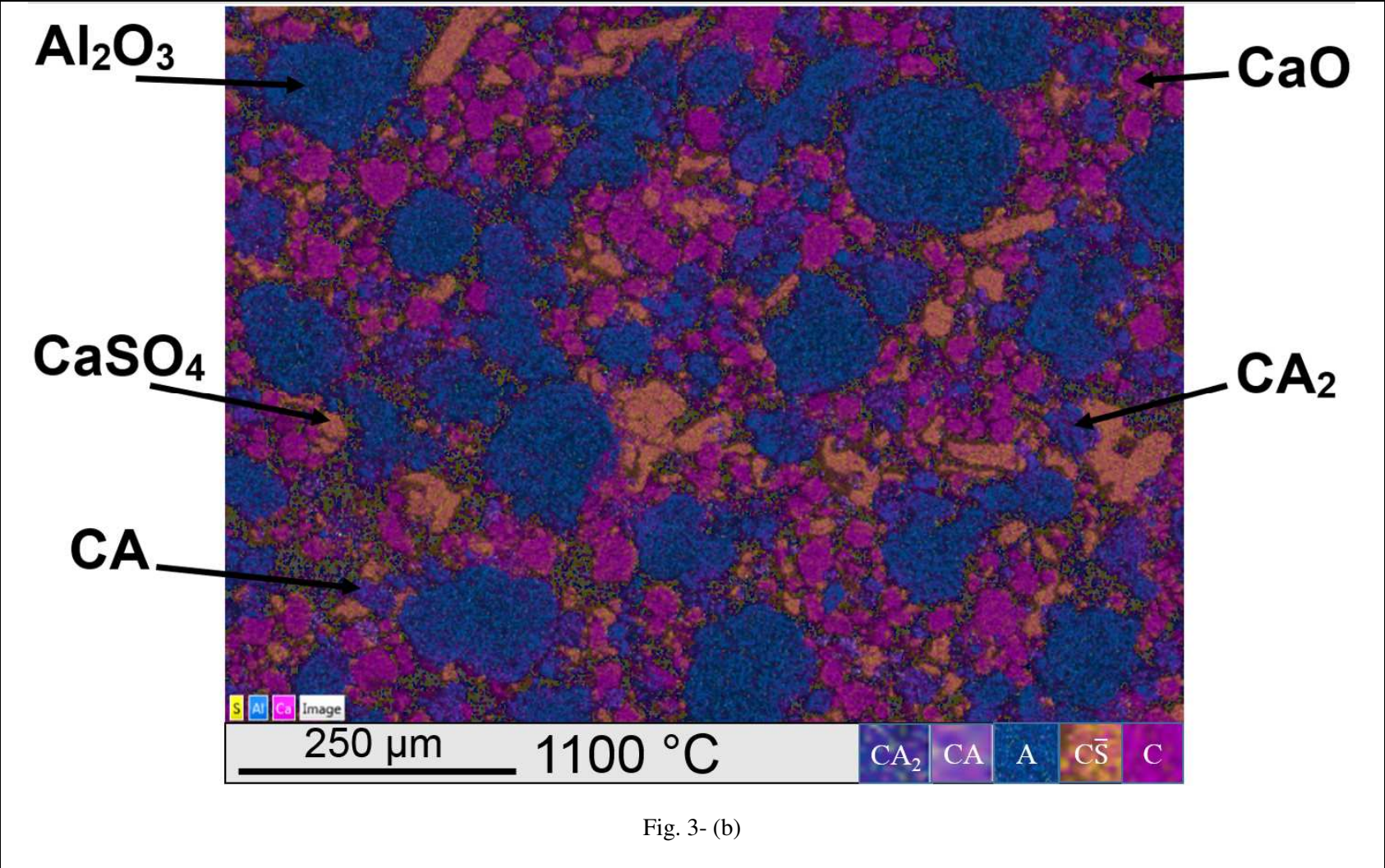
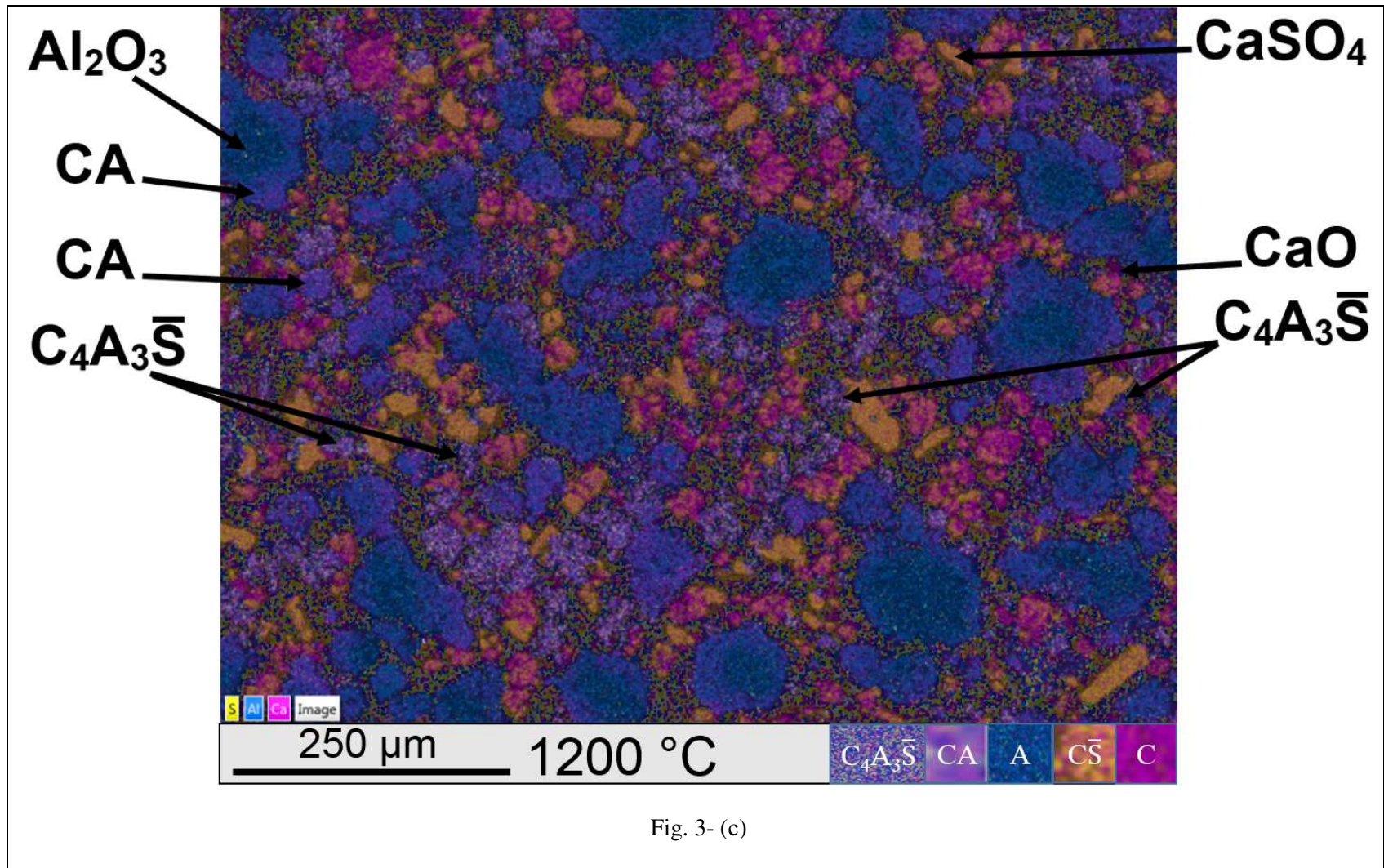


Fig. 3- (b)



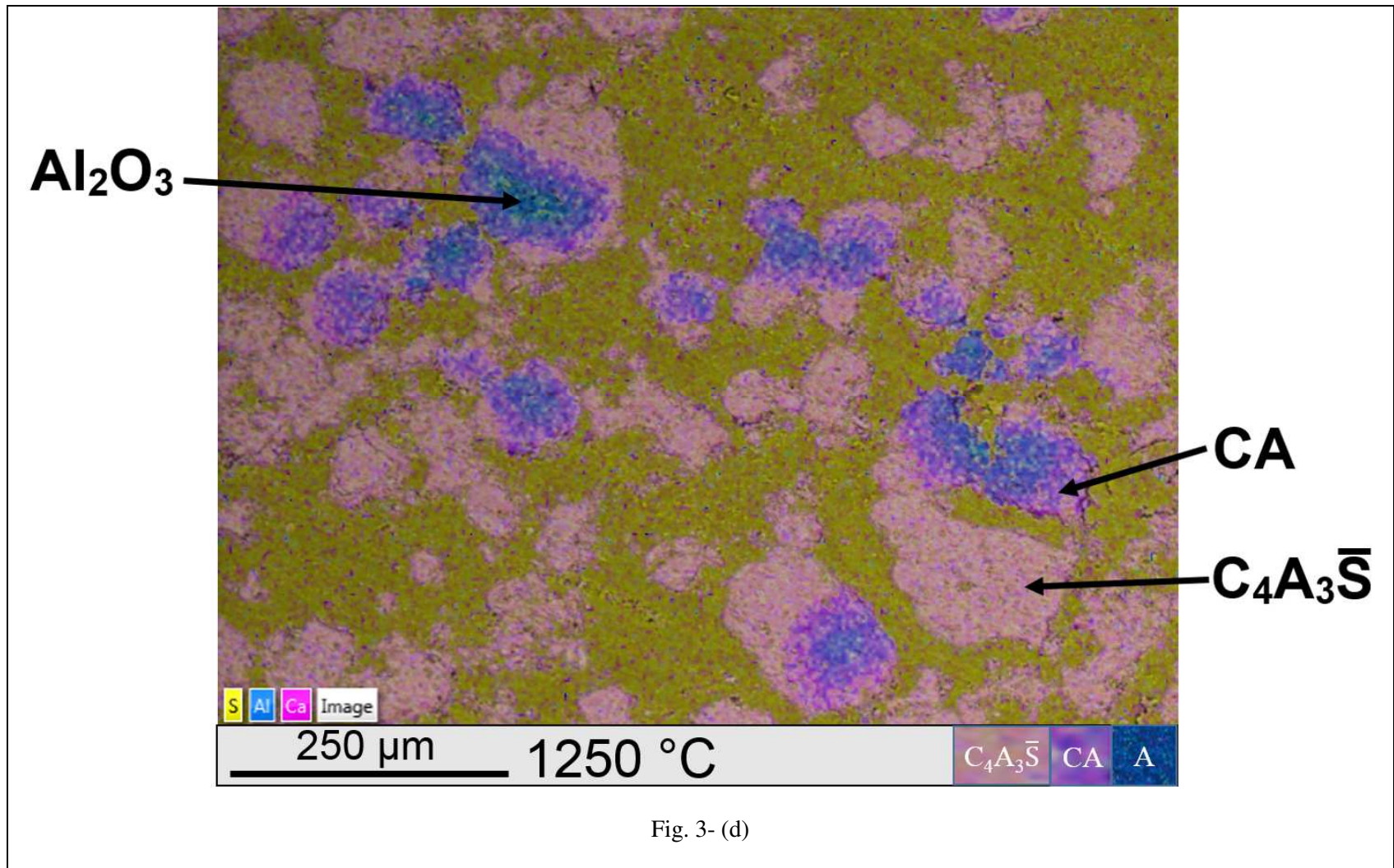


Fig. 3- (d)

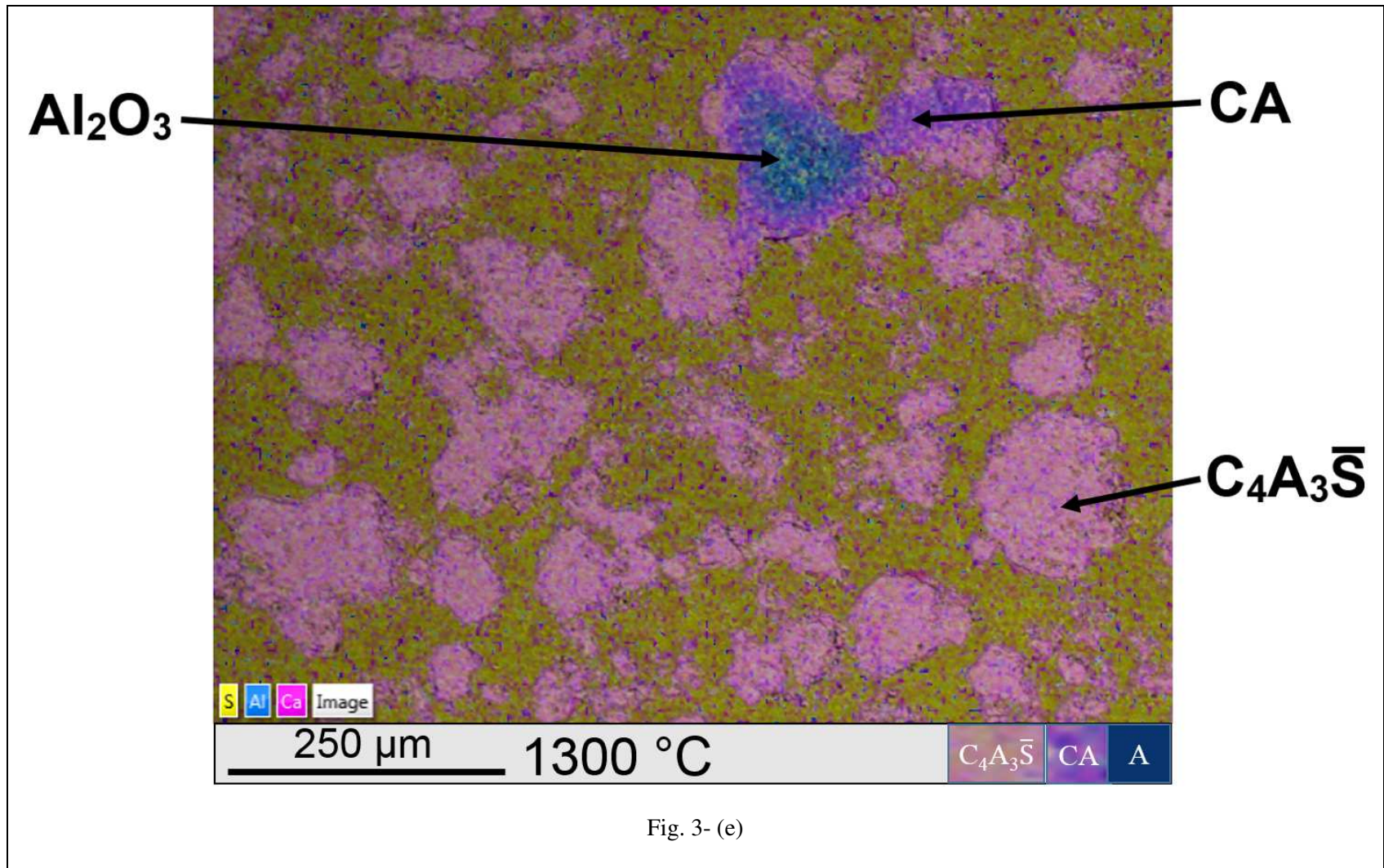


Fig. 3- (e)

Figure. 3

EDS mapping of BSE images (x500)

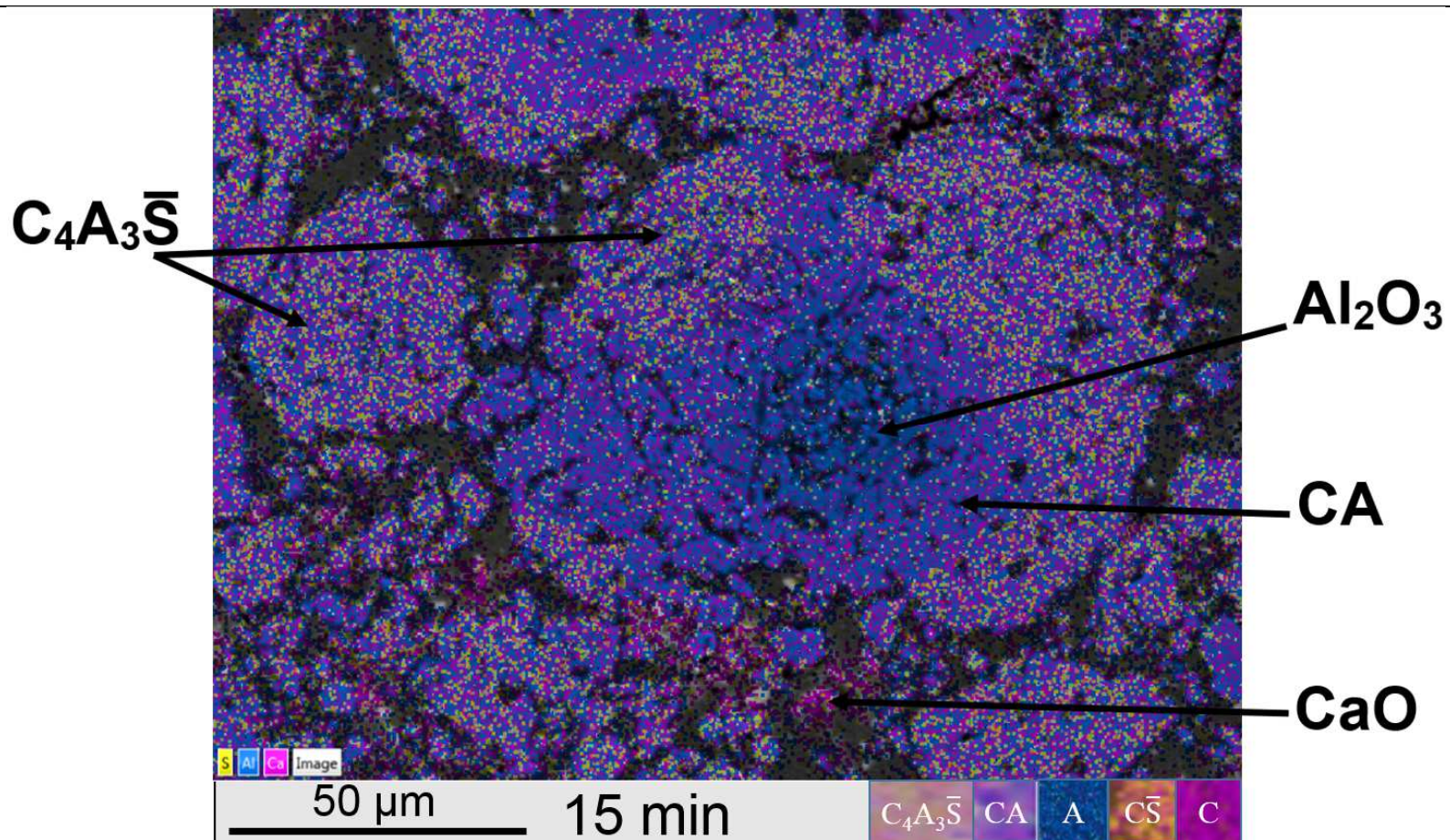
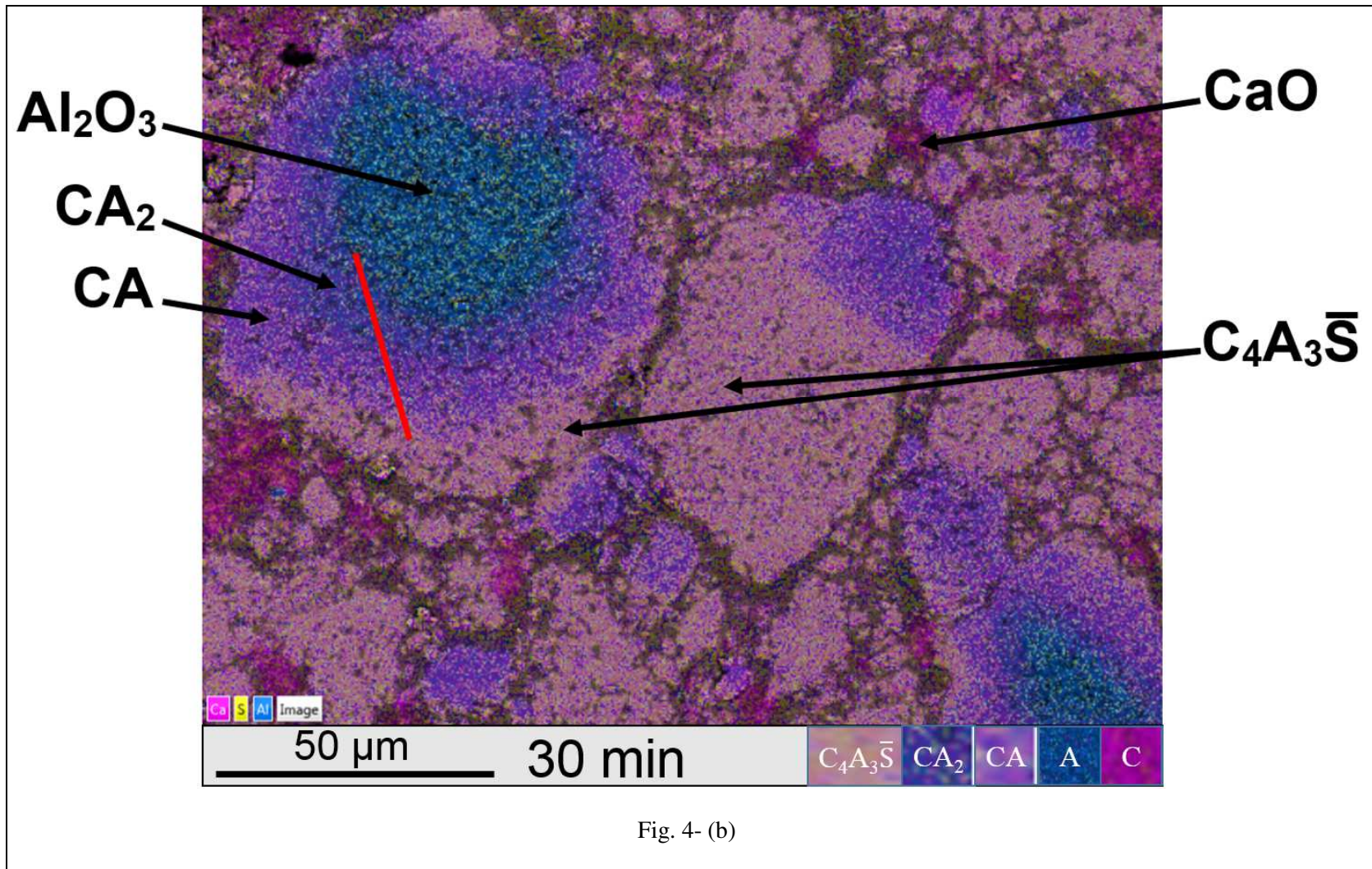


Fig. 4- (a)



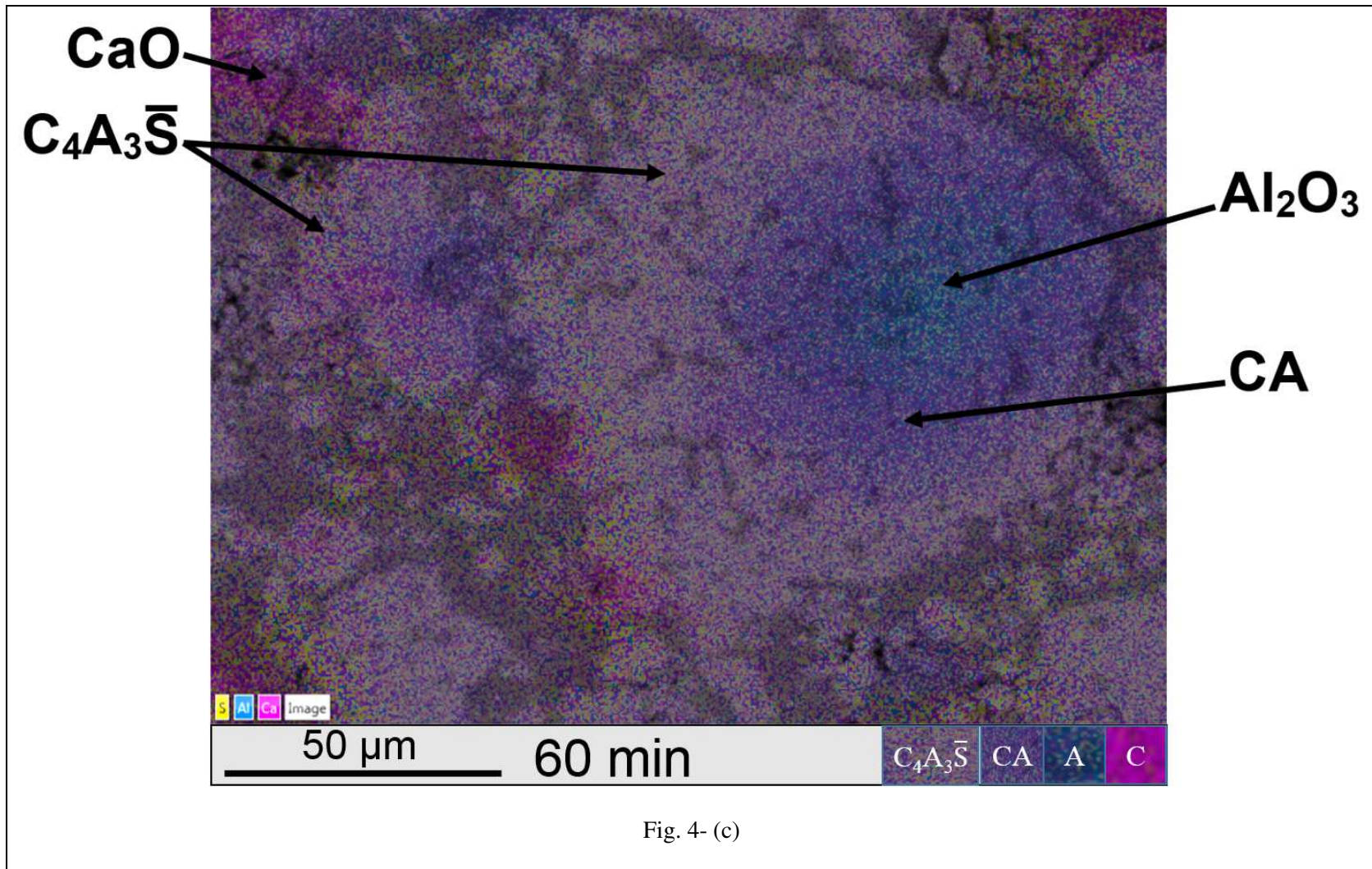
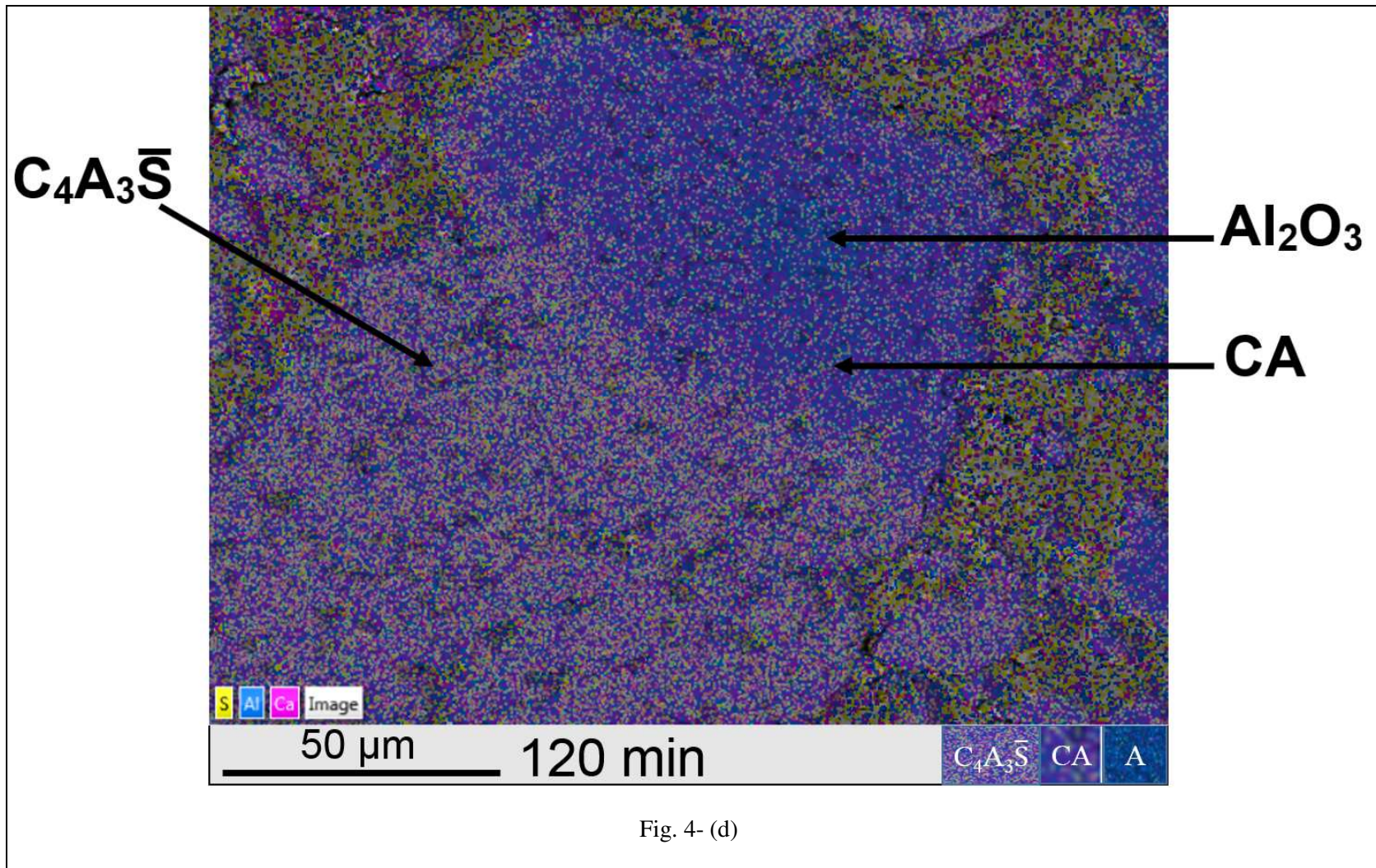
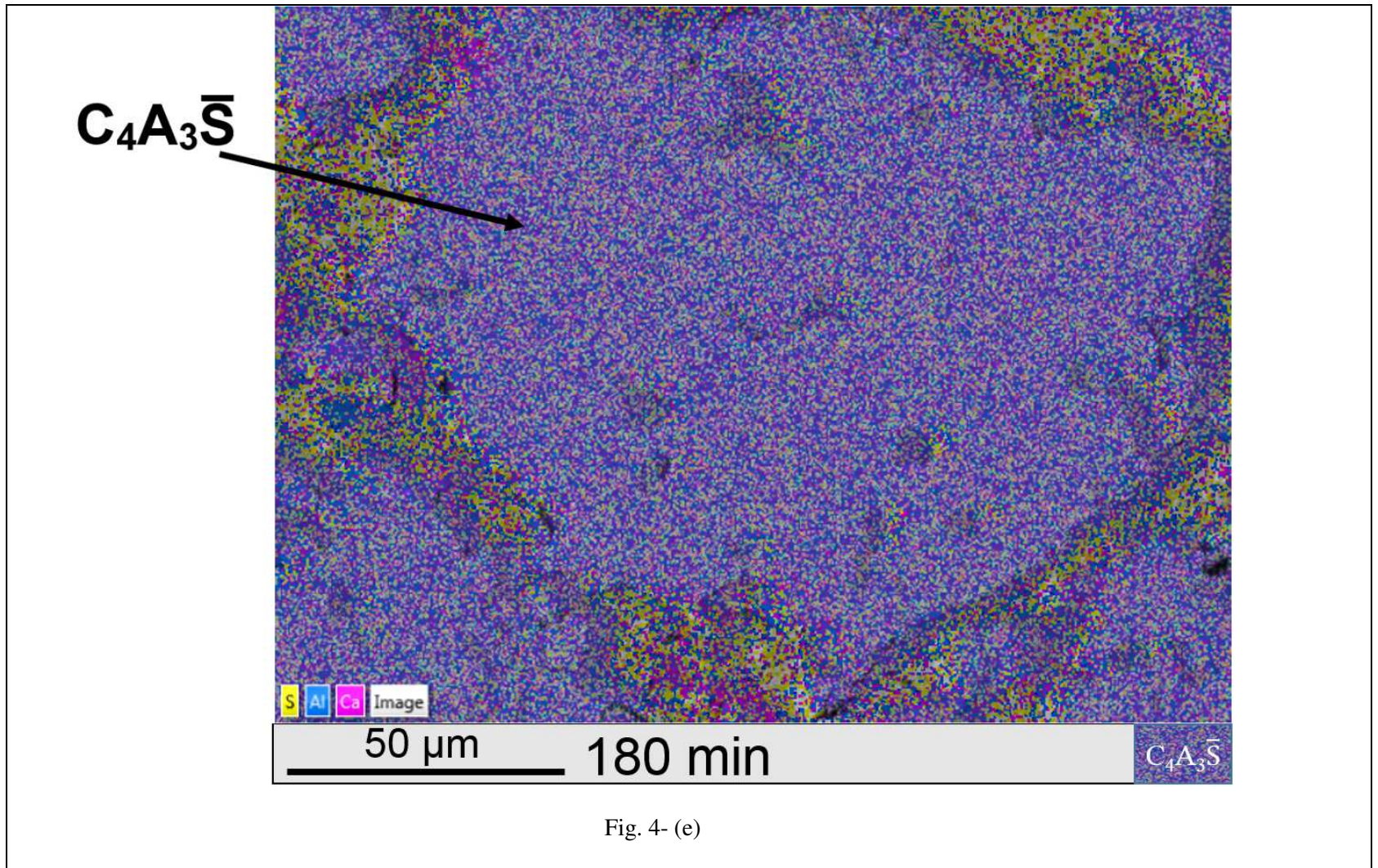


Fig. 4- (c)





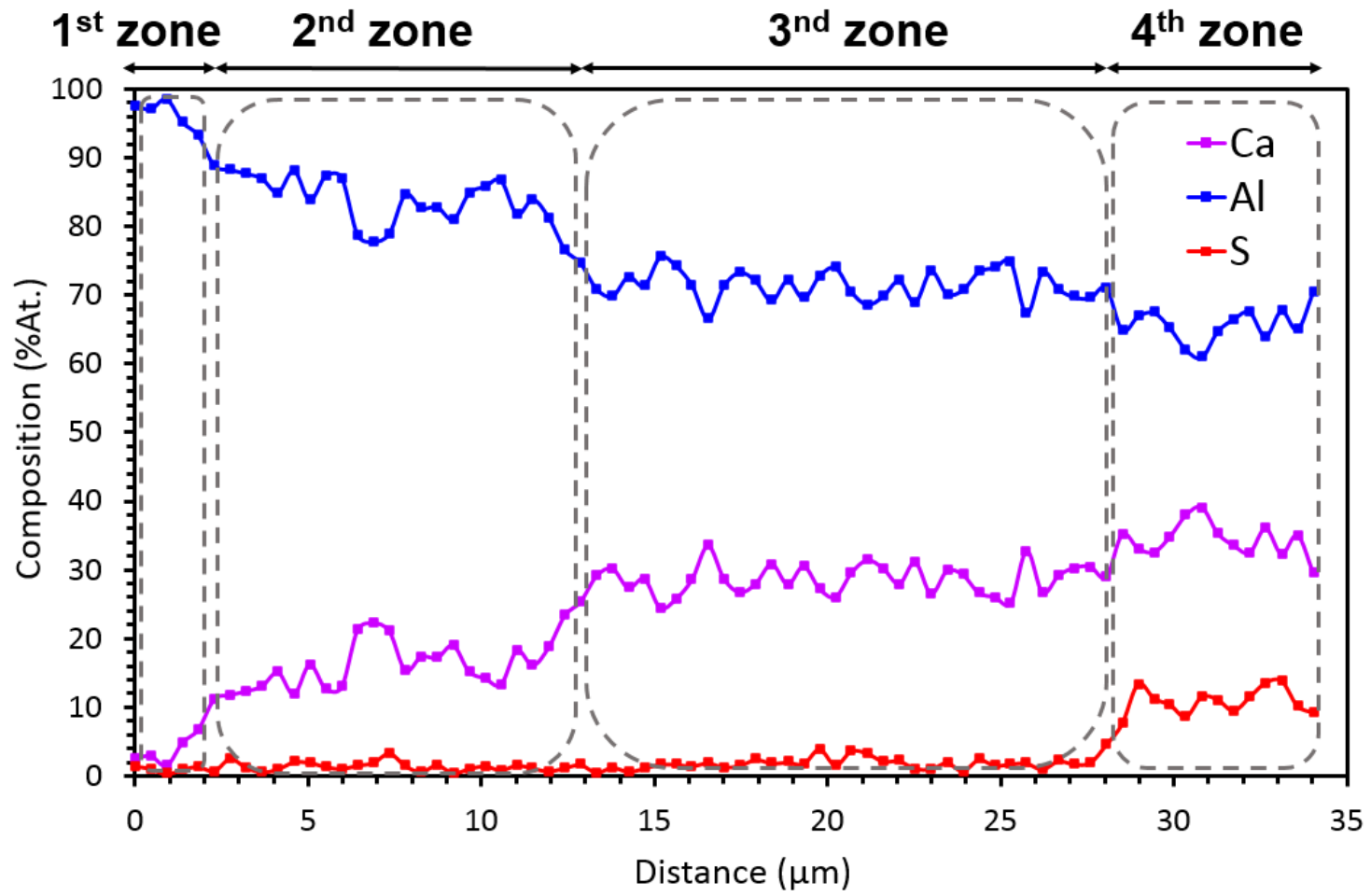


Fig.5- (a)

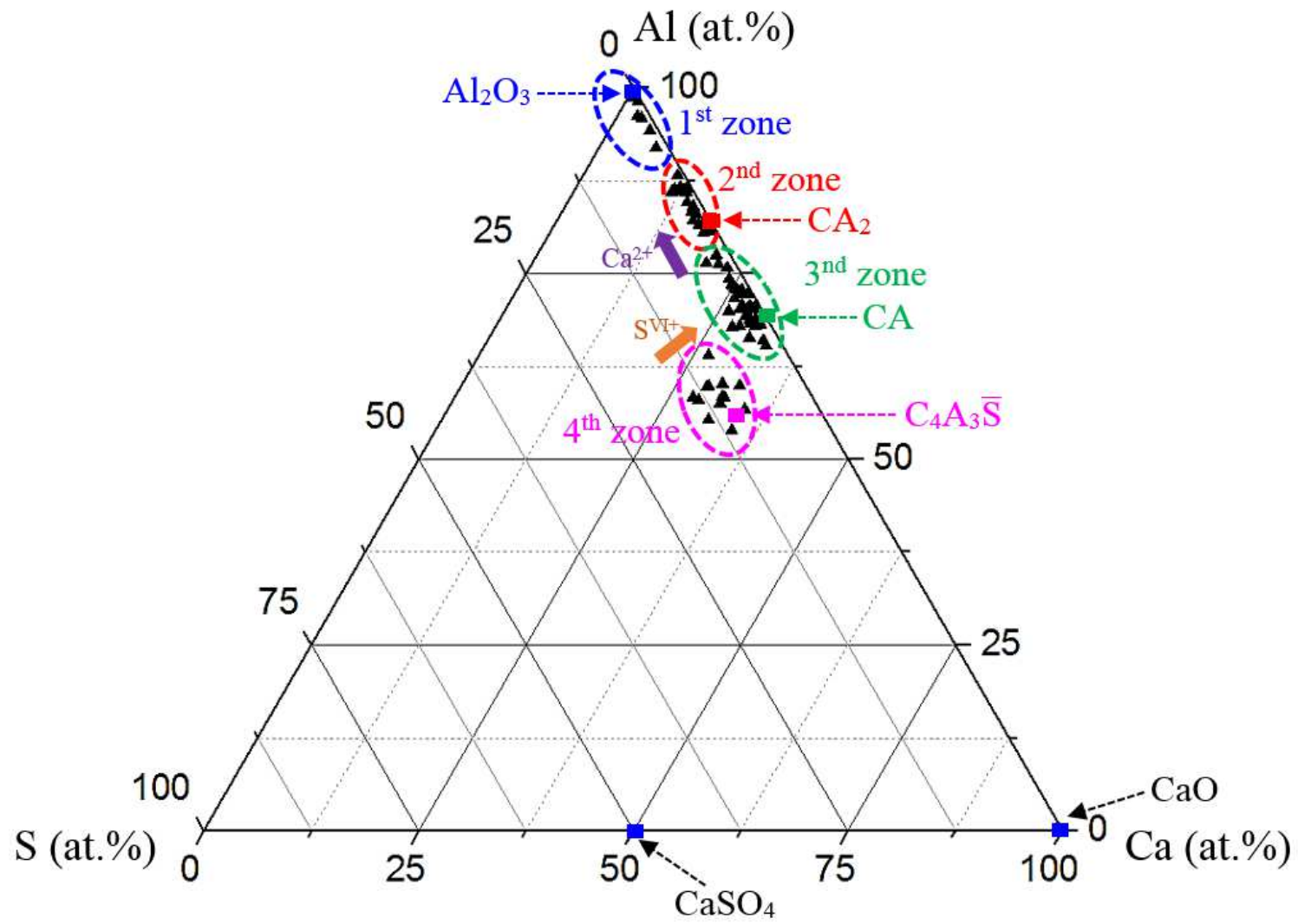


Fig.5- (b)

Figure. 5

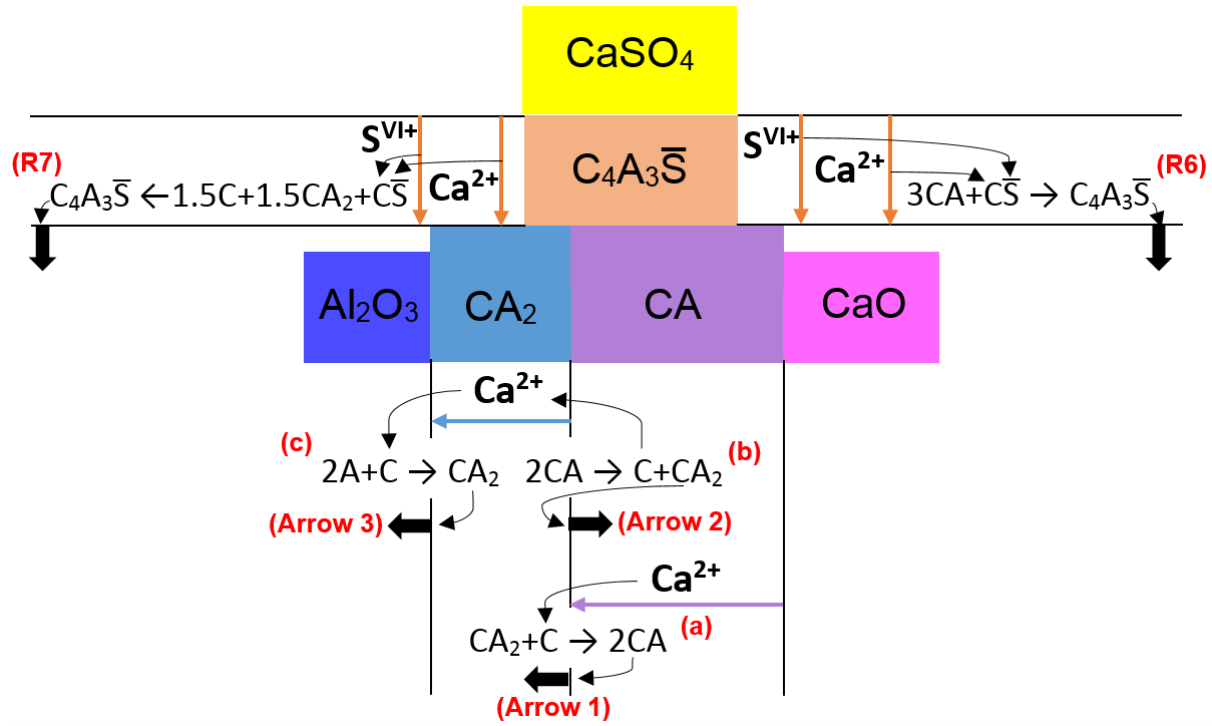


Fig.6- (a)

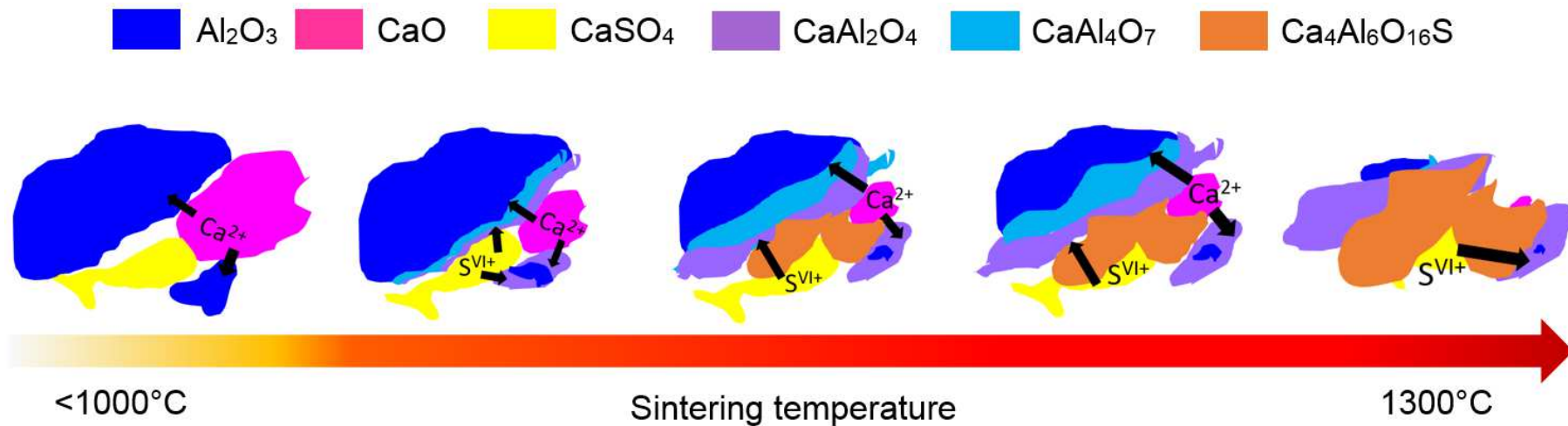


Fig.6- (b)

■ Al_2O_3 ■ CaO ■ CaSO_4 ■ CaAl_2O_4 ■ CaAl_4O_7 ■ $\text{Ca}_4\text{Al}_6\text{O}_{16}\text{S}$

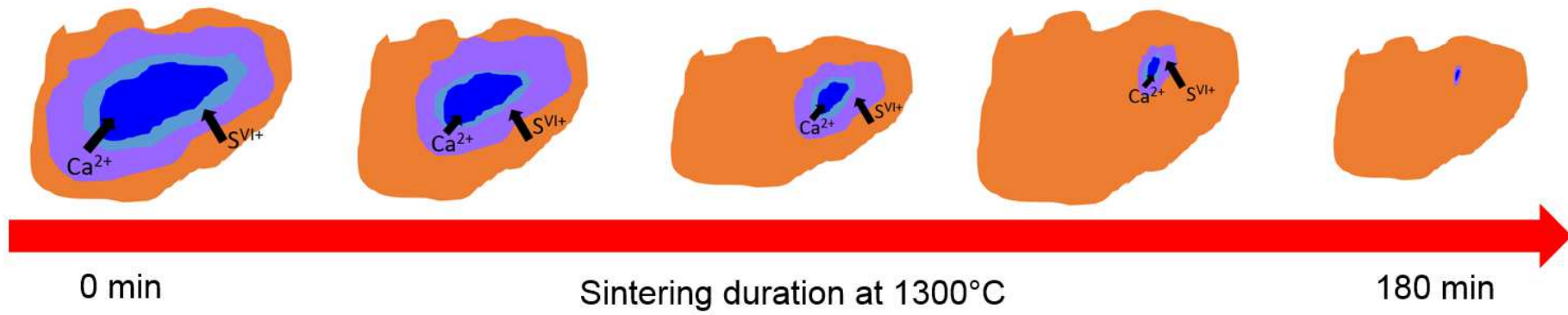
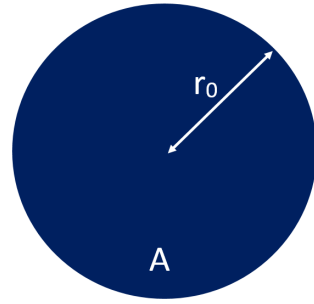
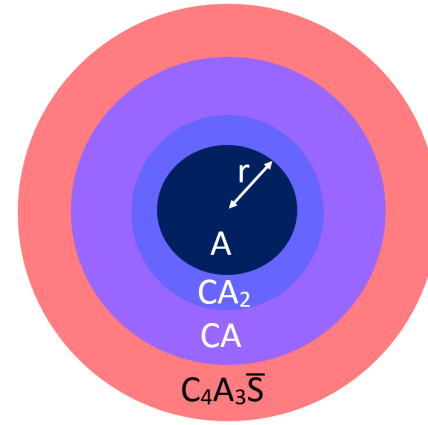


Fig.6- (c)

Figure 6



t_0



$t_0 + \Delta t$

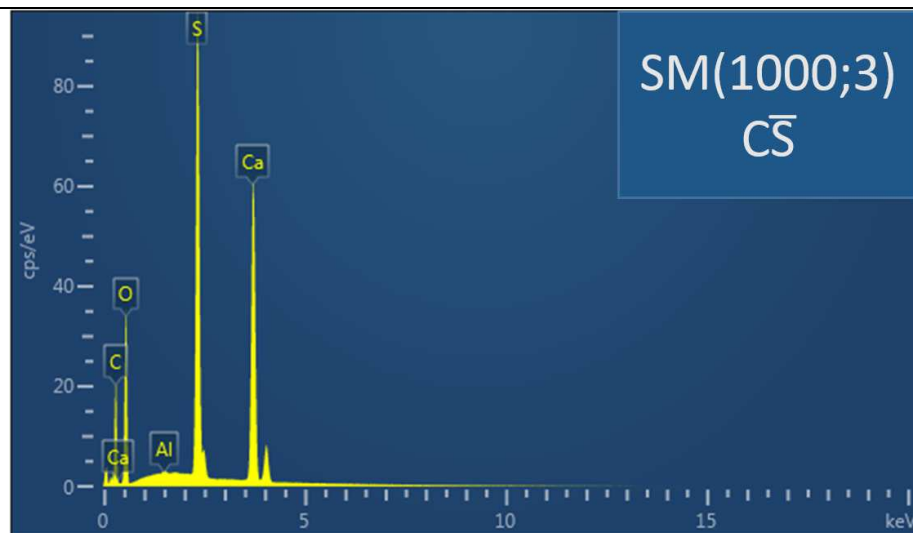
Figure. 7

Appendix A – typical EDS spectra of samples shown in fig. 3 and fig. 4.

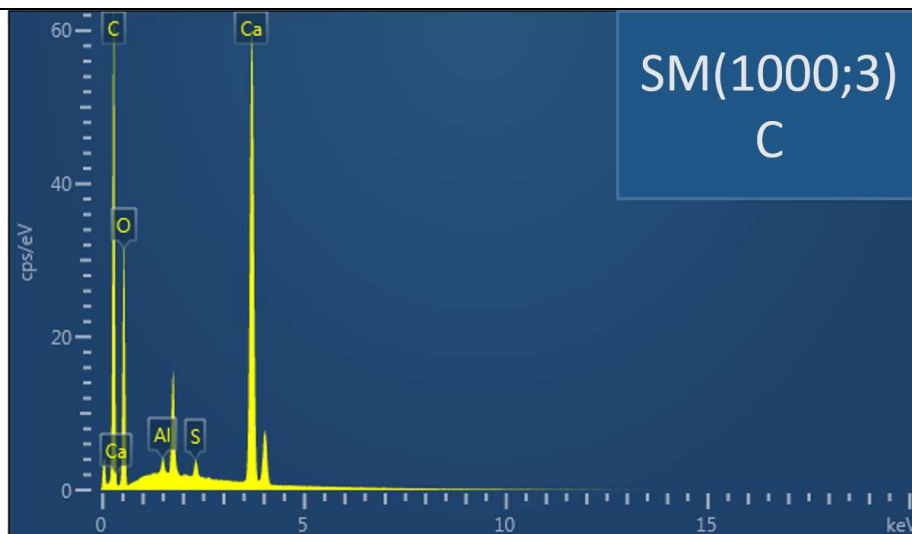
SM(1000;3)



SM(1000;3)
A

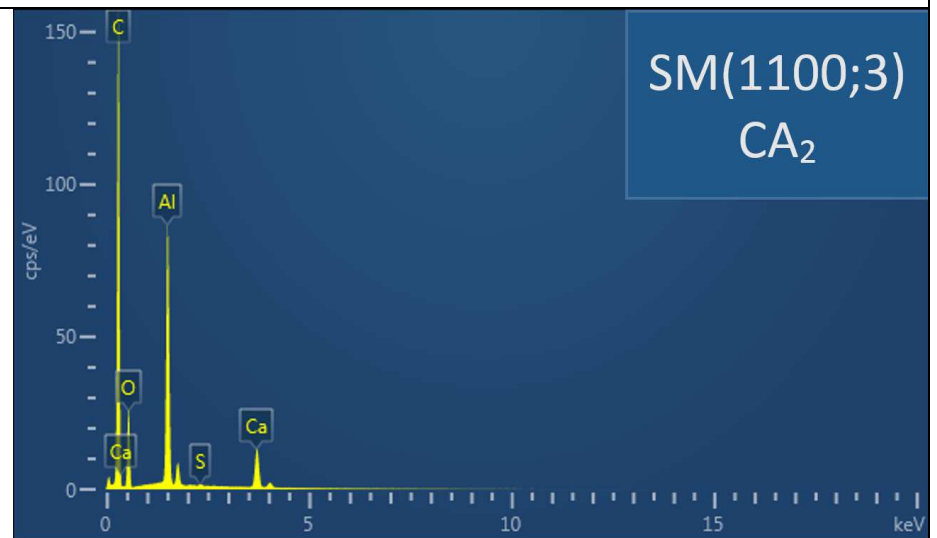
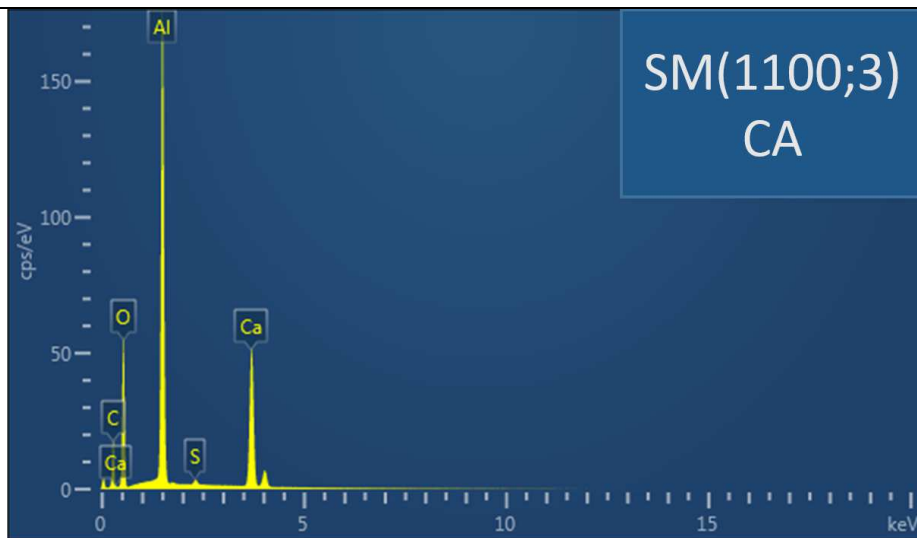
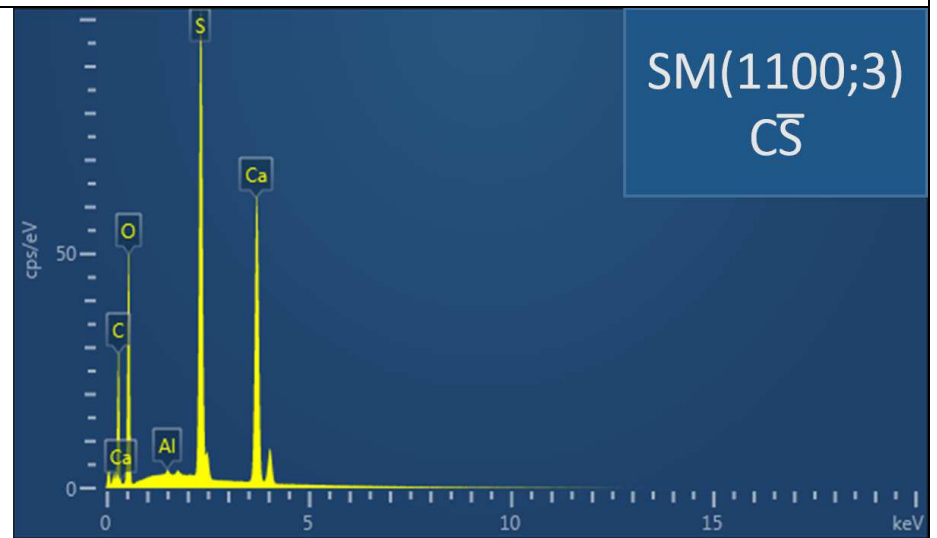


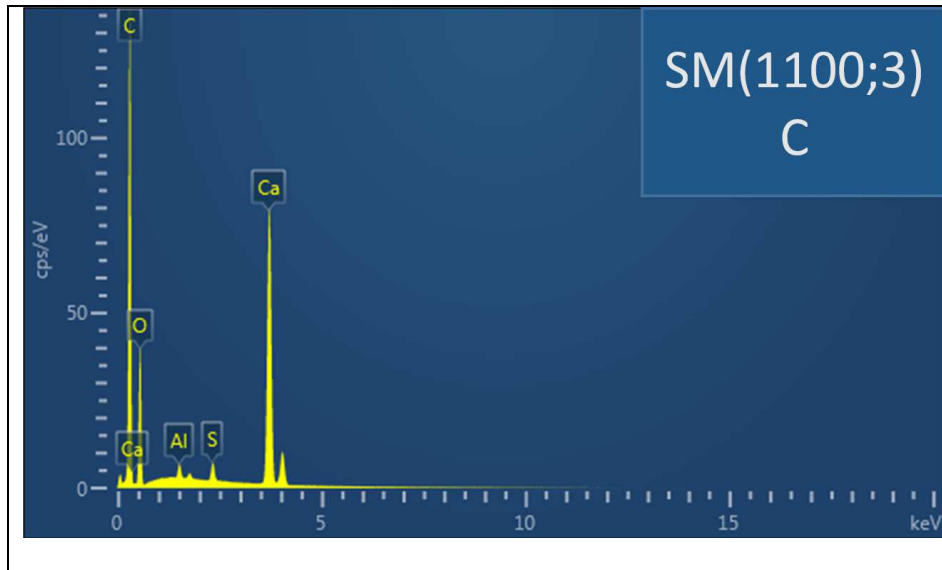
SM(1000;3)
C̄



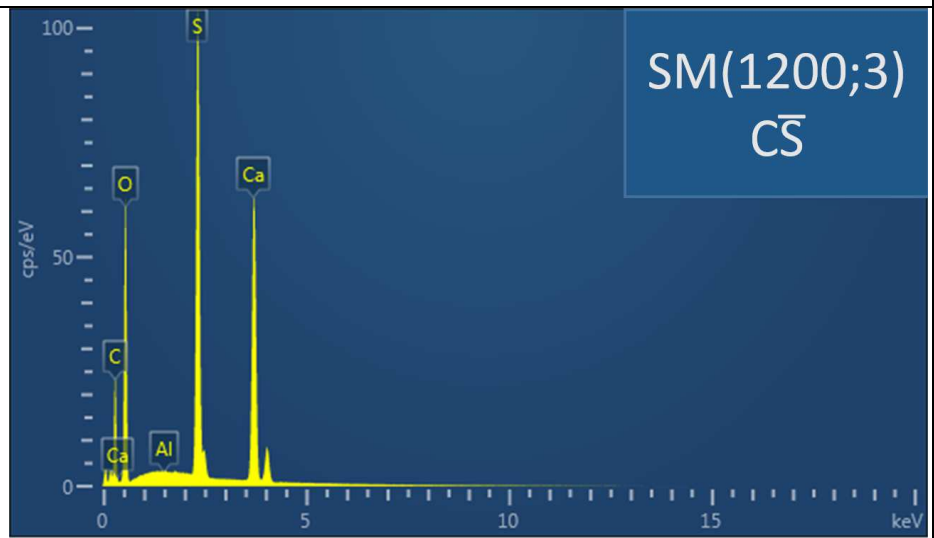
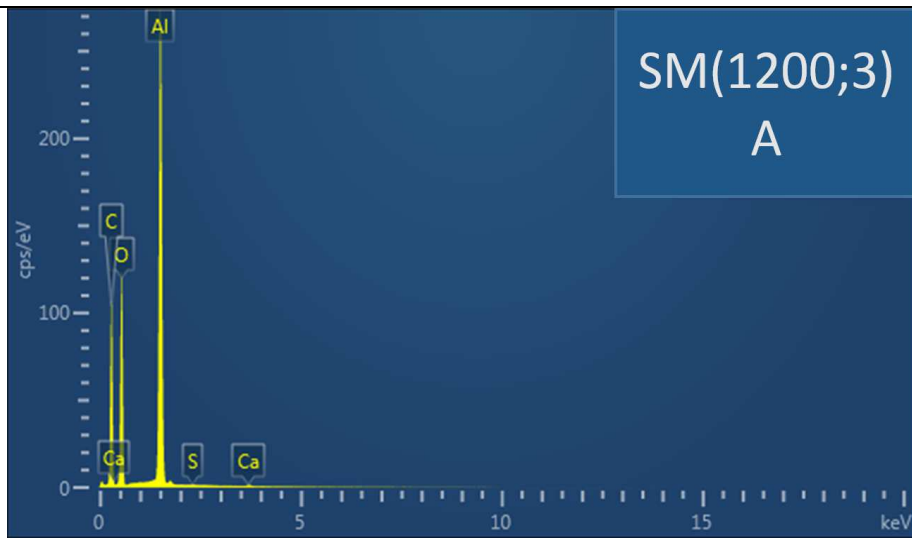
SM(1000;3)
C

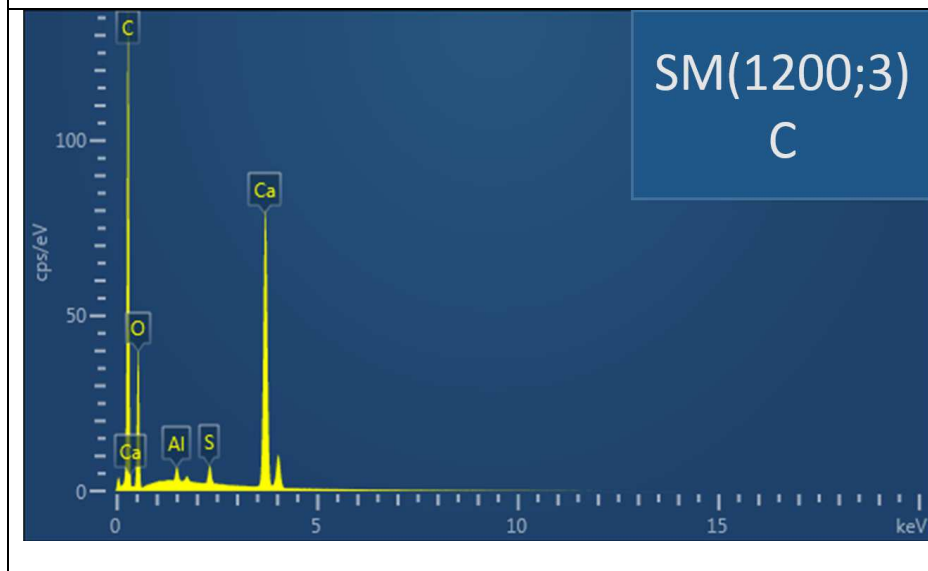
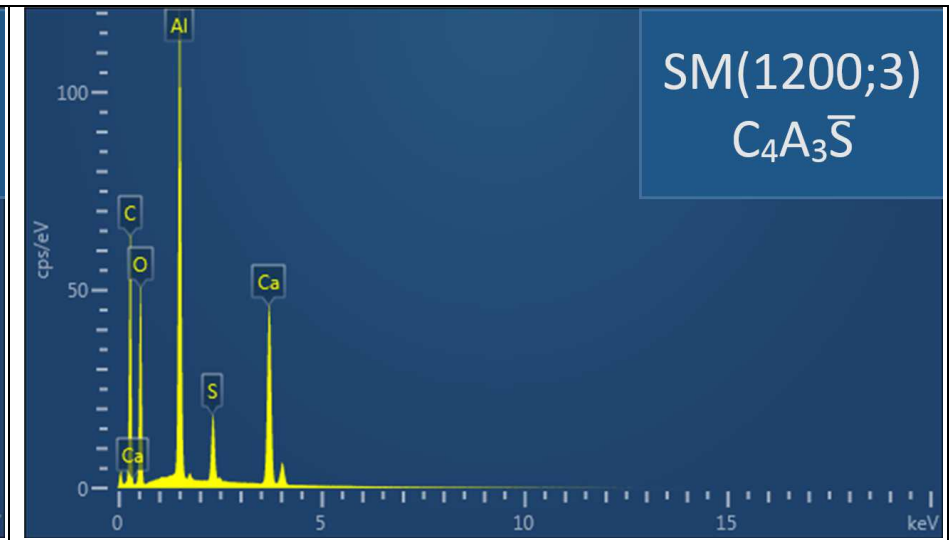
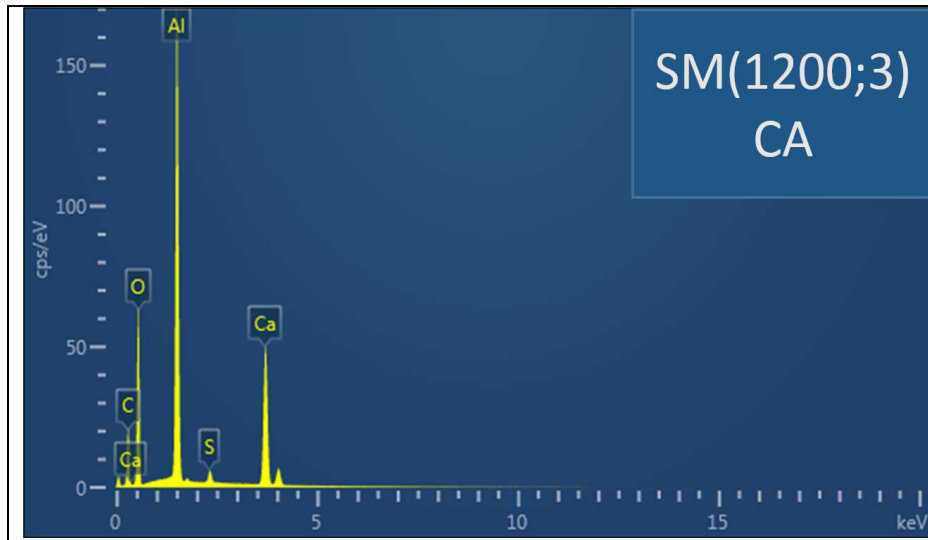
SM(1100;3)



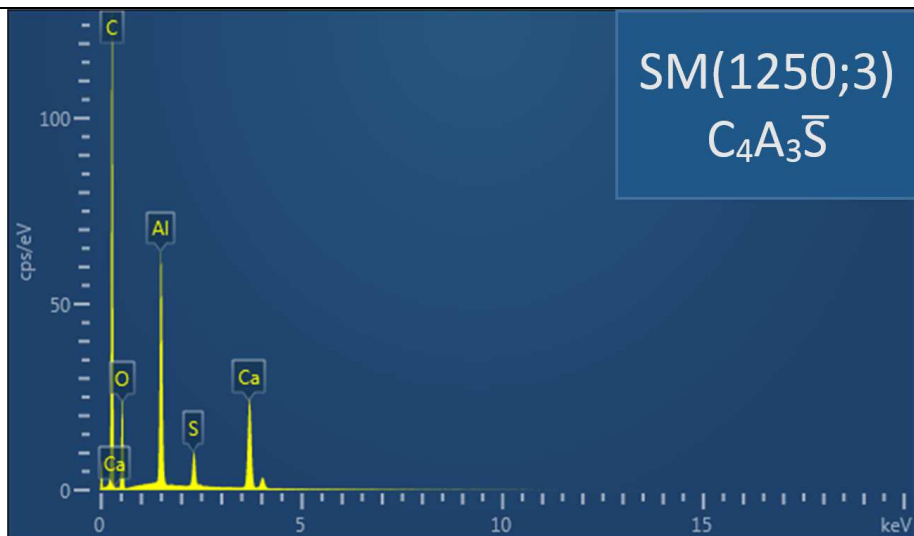
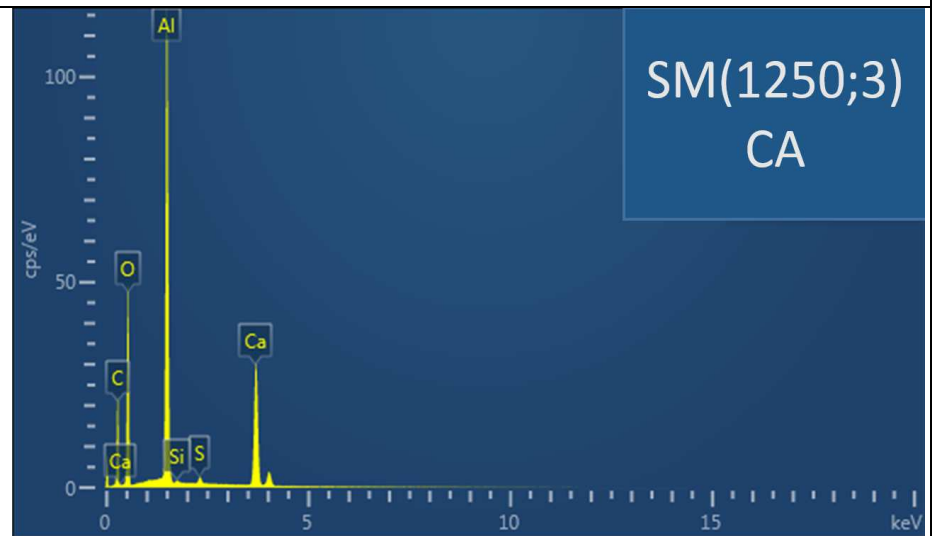


SM(1200;3)

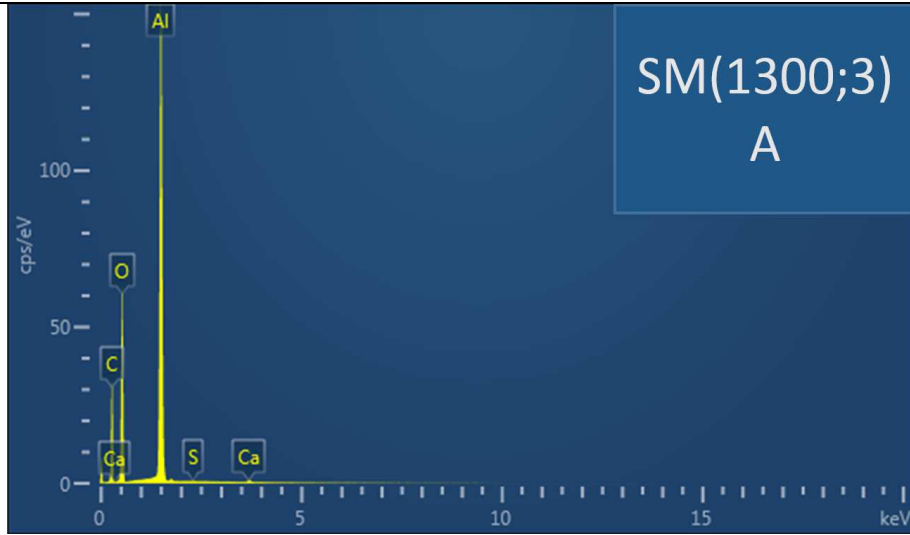




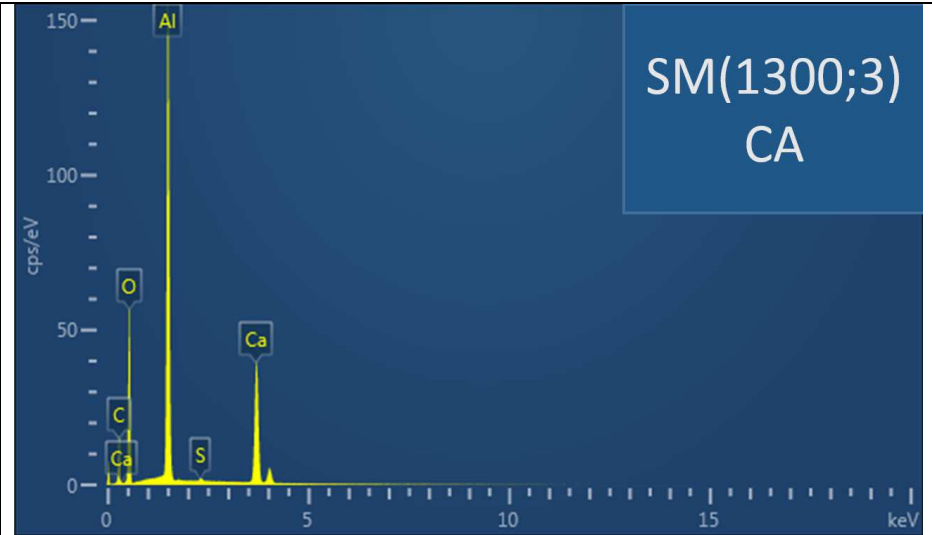
SM(1250;3)



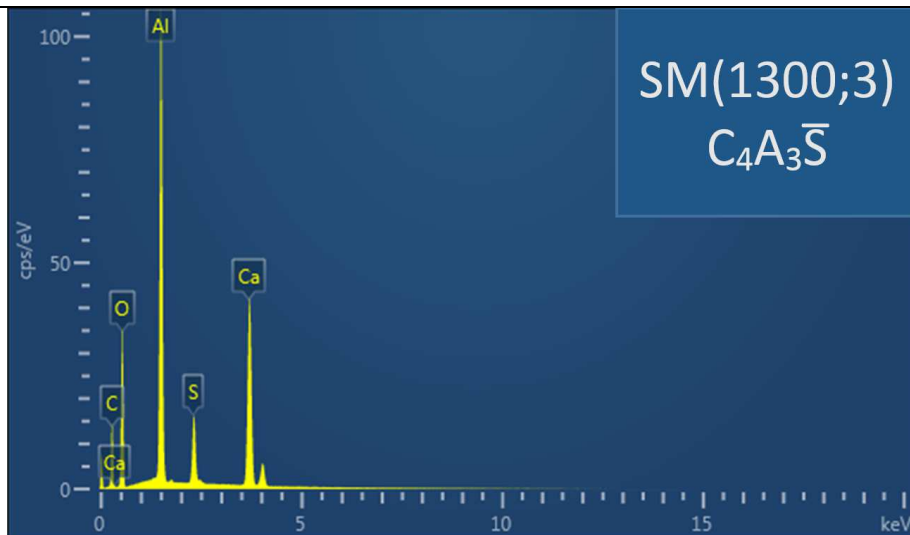
SM(1300;3)



SM(1300;3)
A

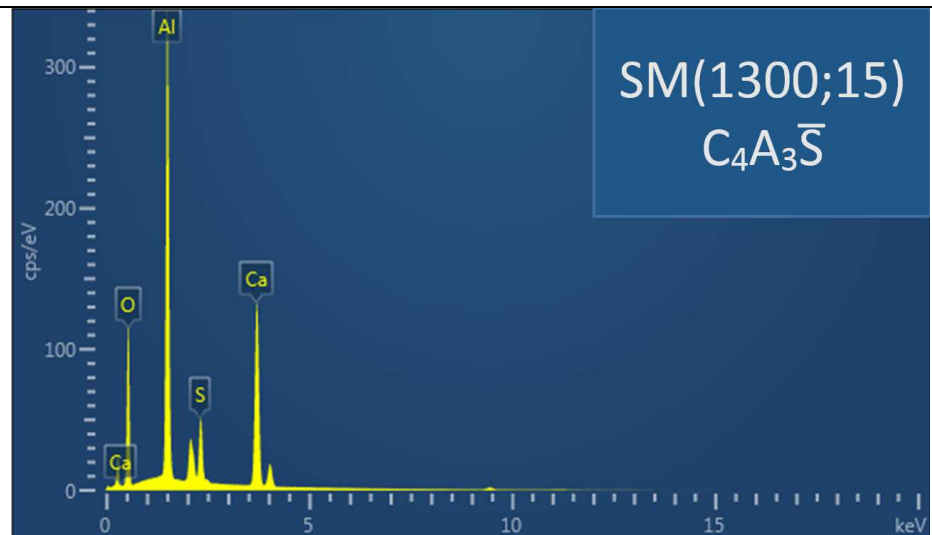
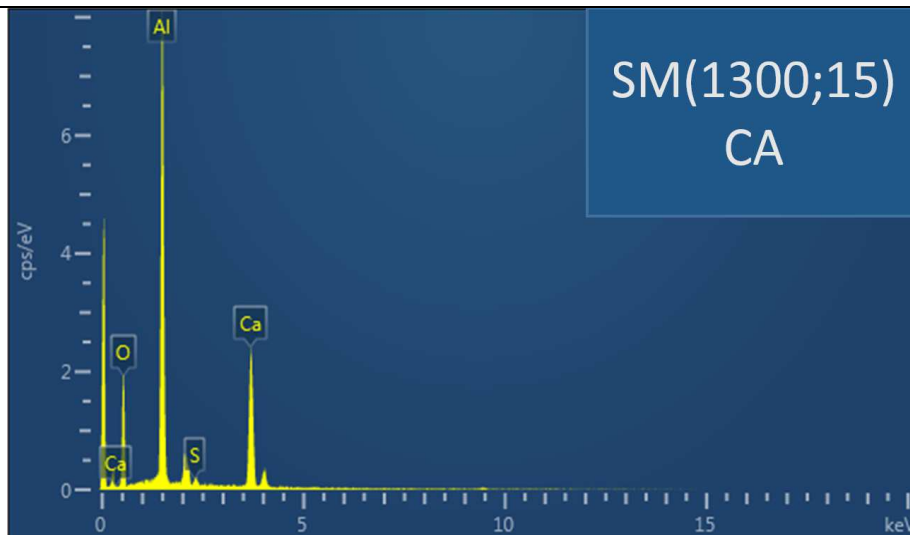
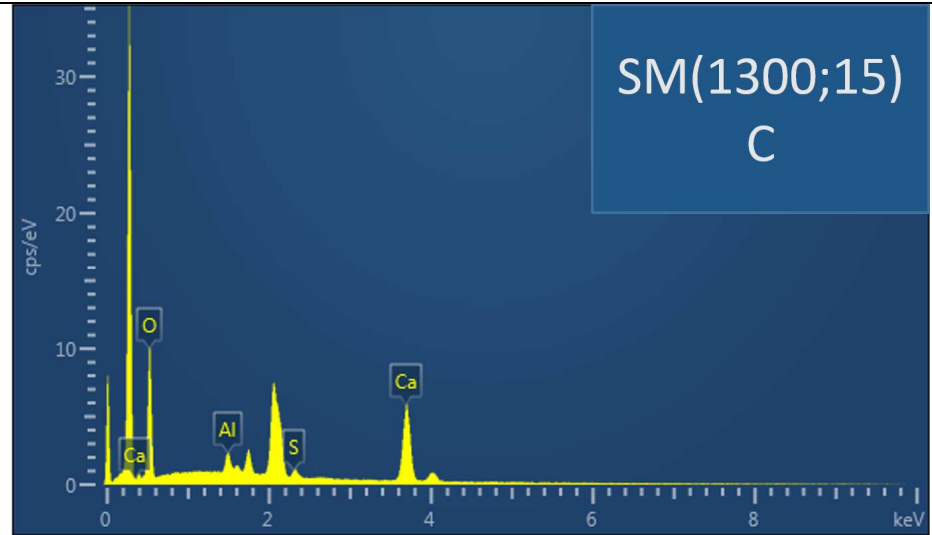


SM(1300;3)
CA

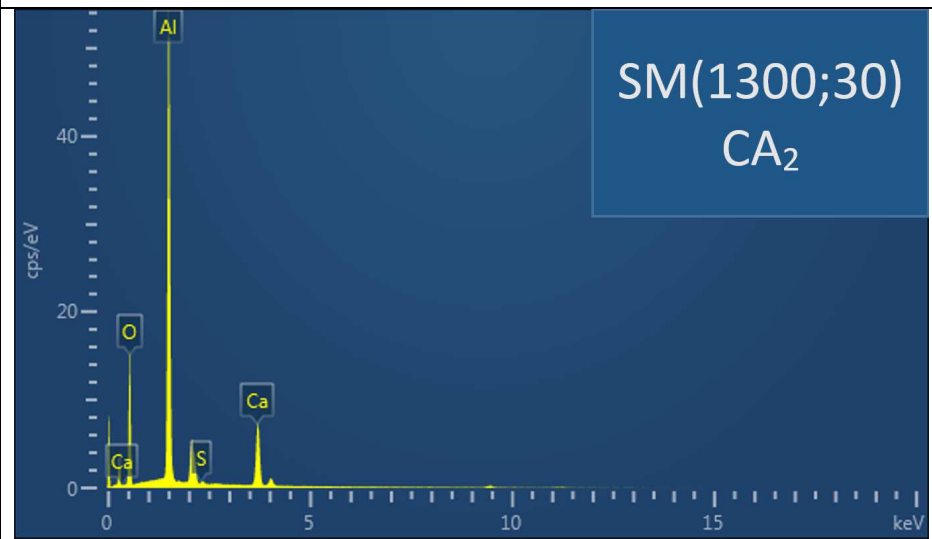
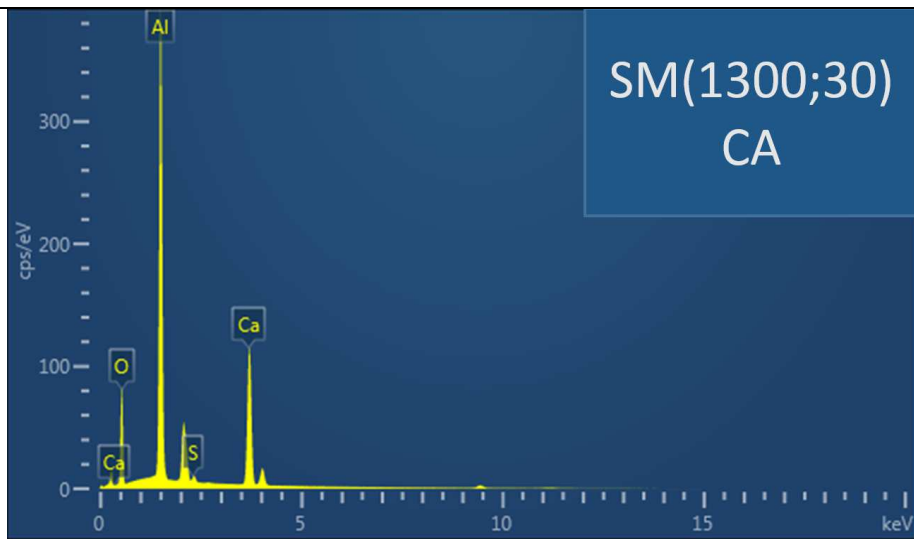
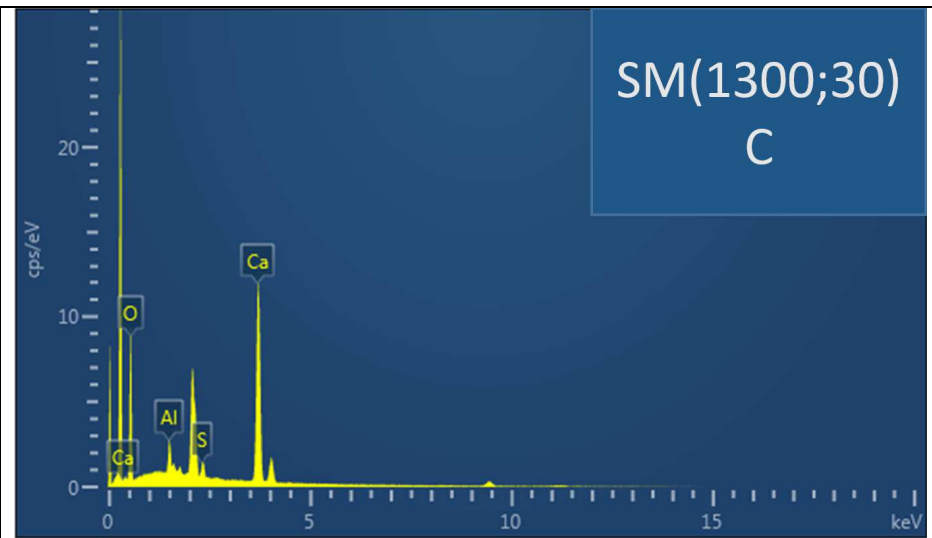
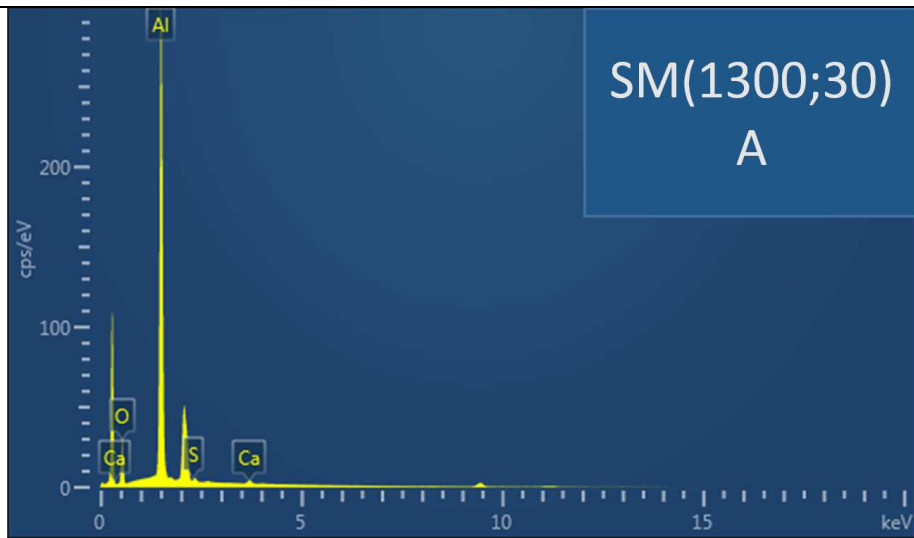


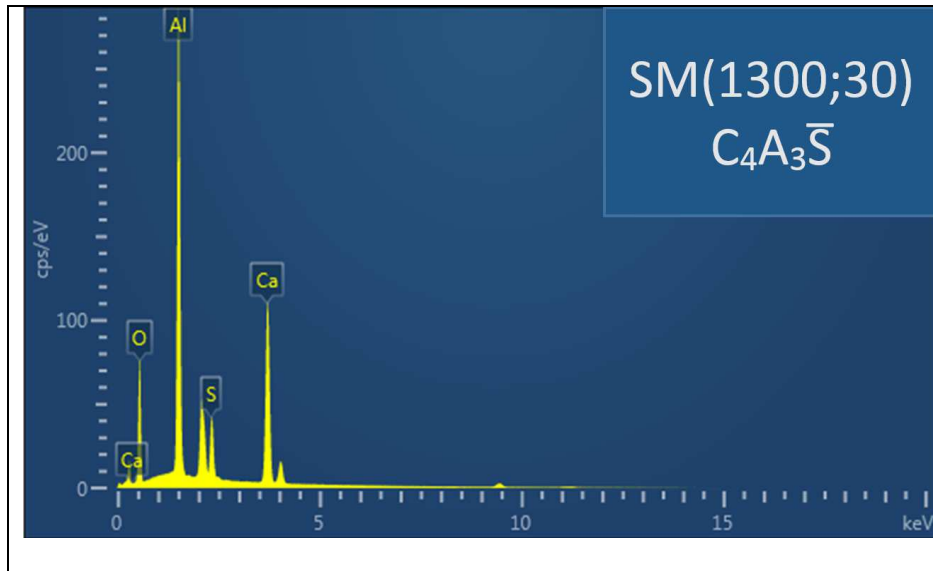
SM(1300;3)
 $C_4A_3\bar{S}$

SM(1300;15)

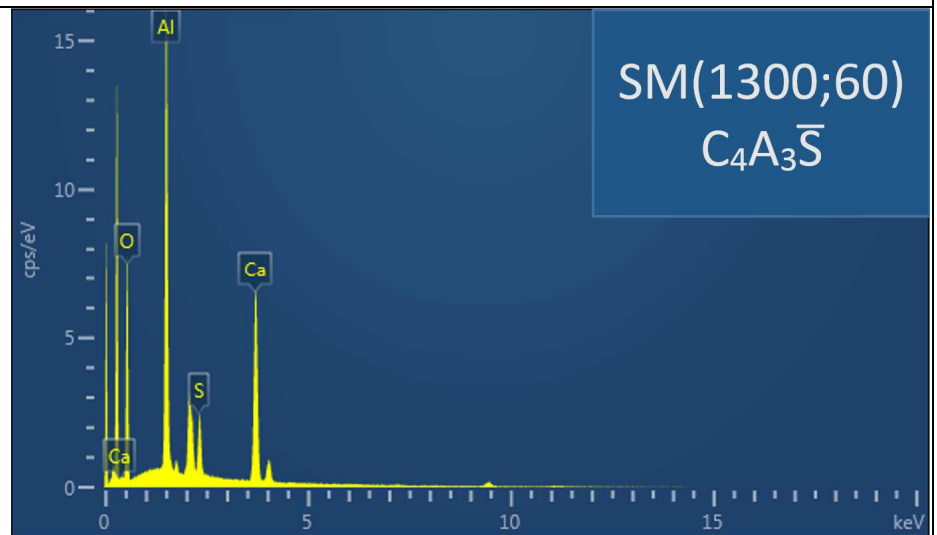
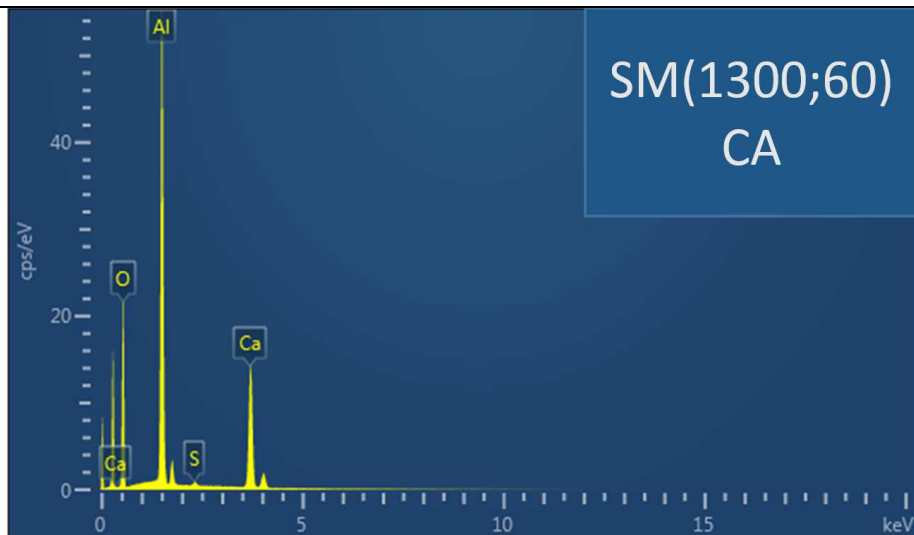
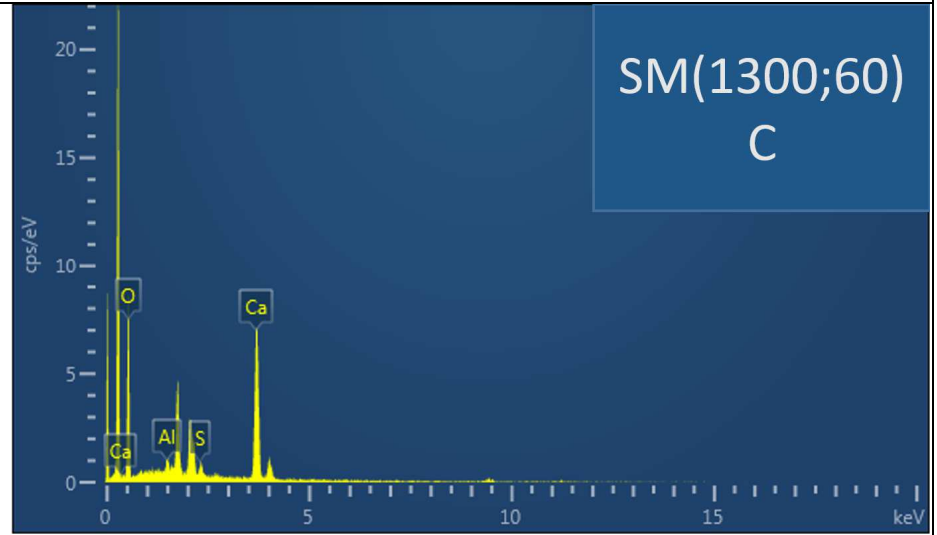


SM(1300;30)

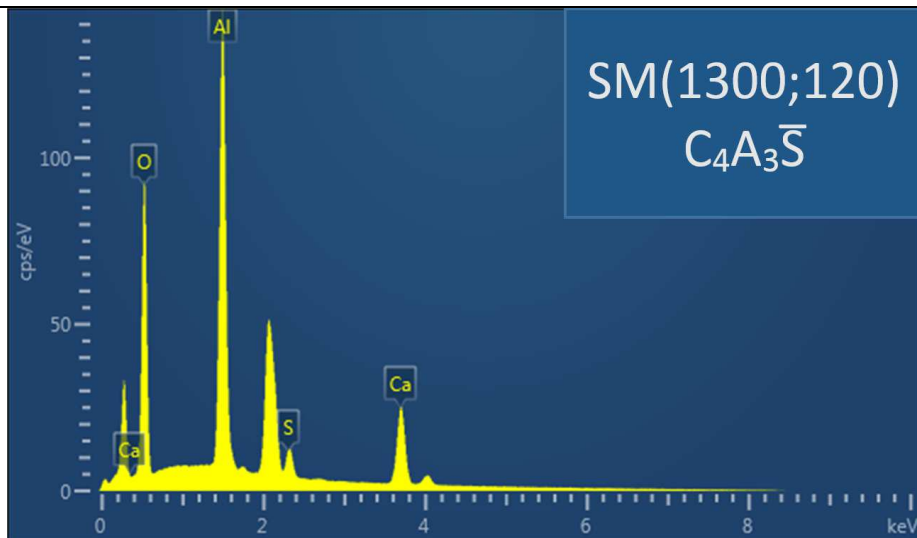
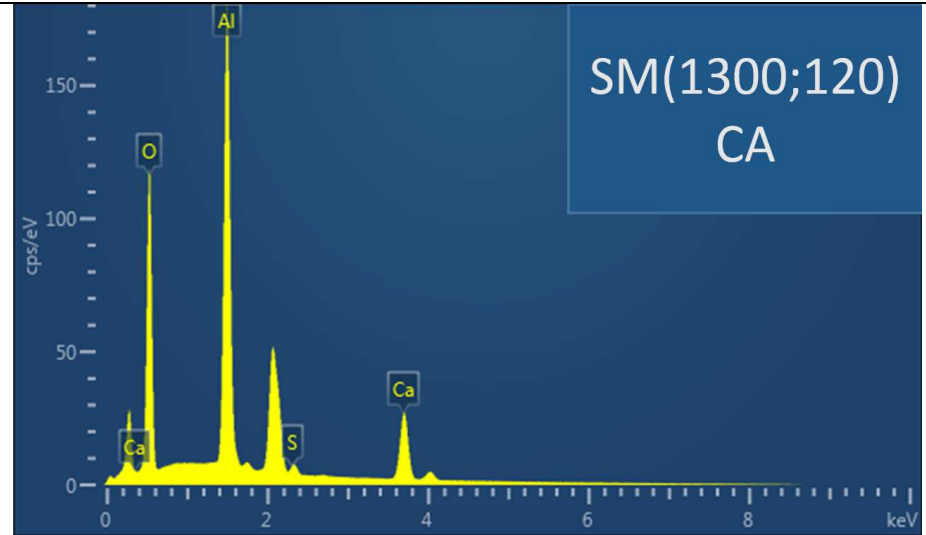
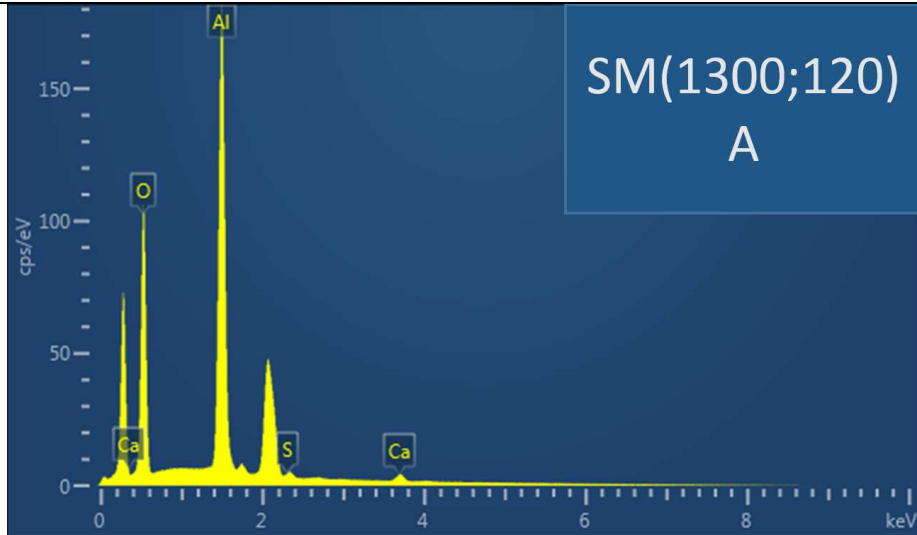




SM(1300;60)



SM(1300;120)



SM(1300;180)

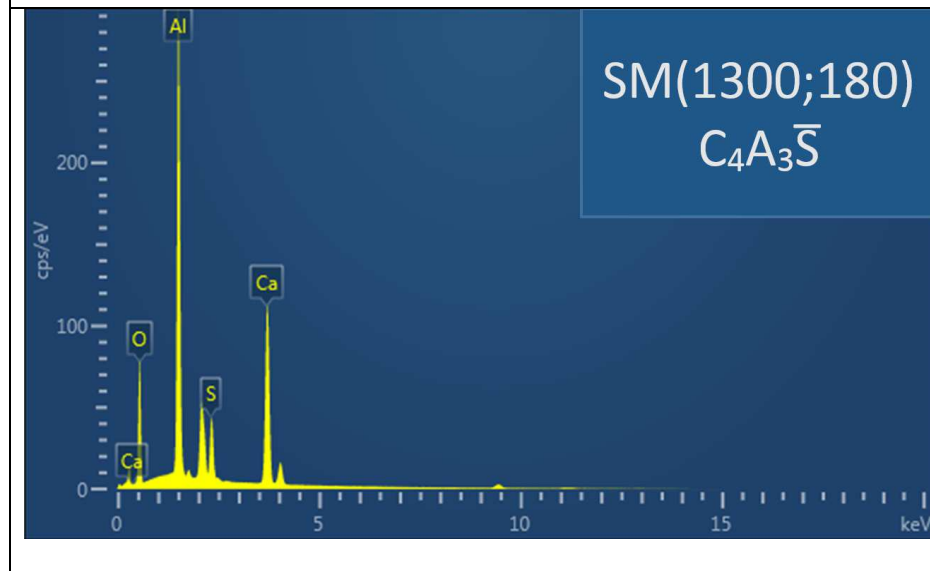


Table captions

Table 1	Some CSA clinkers compositions found in literature.
Table 2	Possible reactions involved during ye'elite formation in different temperature ranges [19]. The cementitious notations are the following: C= CaO, A = Al ₂ O ₃ , \bar{S} = SO ₃ , \bar{C} = CO ₂ , H = H ₂ O
Table 3	Chemical analysis and physical characteristics of the raw materials.
Table 4	Samples identification and corresponding thermal cycle.
Table 5	Polishing steps.
Table 6	ICSD collection codes used for XRD phase identification.

Table 1

Reference	Composition Wt.%					
	Ye'elimité	CA	CA ₂	C ₁₂ A ₇	C ₃ A	Other phases
[6]	50.0	8.0	-	-	-	42.0
[7]	52.1	-	-	1.2	9.4	37.3
[8]	62.8	8.1	3.1	-	-	26.0
[9]	68.1	3.2	0.7	1.4	-	26.6
[10]	50.0	-	-	-	< 8.0	42.0
[11]	57.0	15.0	-	1.0	-	27.0
[12]	68.1	7.8	1.2	-	3.4	19.5

Table 2

Solid-state reaction	Temperature range
$\text{C}\bar{\text{S}}\text{H}_2 \rightarrow \text{C}\bar{\text{S}} + 2 \text{H} \quad (\text{R1})$ $\text{C}\bar{\text{C}} \rightarrow \text{C} + \bar{\text{C}} \quad (\text{R2})$	$T < 1000 \text{ }^\circ\text{C}$
$\text{C} + \text{A} \rightarrow \text{CA} \quad (\text{R3})$ $3\text{C} + 3\text{A} + 1\text{C}\bar{\text{S}} \rightarrow \text{C}_4\text{A}_3\bar{\text{S}} \quad (\text{R4})$ $\text{CA} + \text{A} \rightarrow \text{CA}_2 \quad (\text{R5})$	$1000 \text{ }^\circ\text{C} < T < 1100 \text{ }^\circ\text{C}$
$3\text{CA} + 1\text{C}\bar{\text{S}} \rightarrow \text{C}_4\text{A}_3\bar{\text{S}} \quad (\text{R6})$ $3\text{C} + 3\text{CA}_2 + 2 \text{C}\bar{\text{S}} \rightarrow 2\text{C}_4\text{A}_3\bar{\text{S}} \quad (\text{R7})$	$1100 \text{ }^\circ\text{C} < T < 1300 \text{ }^\circ\text{C}$
$\text{C}\bar{\text{S}} \rightarrow \text{C} + \bar{\text{S}} \rightarrow \text{C} + \text{SO}_2^\uparrow + \frac{1}{2}\text{O}_2^\uparrow \quad (\text{R8})$ $\text{C}_4\text{A}_3\bar{\text{S}} \rightarrow \frac{1}{5} \text{C}_{12}\text{A}_7 + \frac{8}{5} \text{CA} + \text{SO}_2^\uparrow + \frac{1}{2} \text{O}_2^\uparrow \quad (\text{R9})$	$T > 1300 \text{ }^\circ\text{C}$

Table 3

Raw material		Alumina	Gypsum	Calcium carbonate
Mineralogical analysis ^(a)		Al ₂ O ₃	CaSO ₄ .2H ₂ O	CaCO ₃
Real density ^(b) (g/cm ³)		3.08	2.30	2.67
Specific surface BET ^(c) (m ² /g)		0.58	4.19	0.22
Particle size ^(d)	d ₁₀ (μm)	3.11	9.92	4.70
	d ₅₀ (μm)	5.62	23.08	10.83
	d ₉₀ (μm)	11.38	45.32	24.16
Chemical analysis (wt.%) ^(e)	Al ₂ O ₃	99.869	0.030	-
	Fe ₂ O ₃	0.046	-	0.057
	SiO ₂	-	0.042	0.039
	SO ₃	-	46.504	0.062
	CaO	-	33.777	56.029
	SrO	-	0.017	0.033
	Ga ₂ O ₃	0.011	-	-
	Ignition loss	0.07	19.63	43.78

^(a) XRD phase identification

^(b) Helium pycnometry

^(c) BET analysis

^(d) Laser diffraction granulometry

^(e) XRF analysis

Table 4

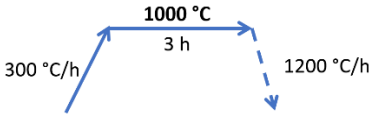
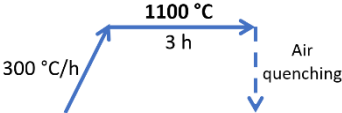
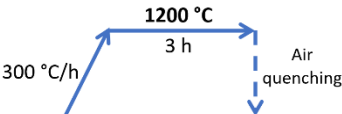
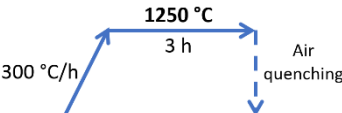
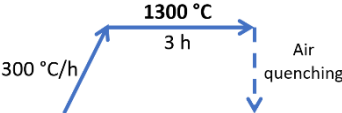
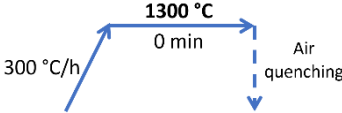
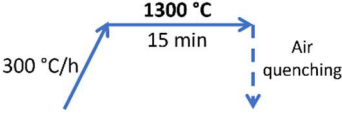
Samples identification	Thermal cycle
SM(1000;3)	 <p>300 °C/h → 1000 °C (3 h) → 1200 °C/h</p>
SM(1100;3)	 <p>300 °C/h → 1100 °C (3 h) → Air quenching</p>
SM(1200;3)	 <p>300 °C/h → 1200 °C (3 h) → Air quenching</p>
SM(1250;3)	 <p>300 °C/h → 1250 °C (3 h) → Air quenching</p>
SM(1300;3)	 <p>300 °C/h → 1300 °C (3 h) → Air quenching</p>
SM(1300;0)	 <p>300 °C/h → 1300 °C (0 min) → Air quenching</p>
SM(1300;15)	 <p>300 °C/h → 1300 °C (15 min) → Air quenching</p>
SM(1300;30)	 <p>300 °C/h → 1300 °C (30 min) → Air quenching</p>
SM(1300;60)	 <p>300 °C/h → 1300 °C (60 min) → Air quenching</p>
SM(1300;120)	 <p>300 °C/h → 1300 °C (120 min) → Air quenching</p>
SM(1300;180)	 <p>300 °C/h → 1300 °C (180 min) → Air quenching</p>

Table 5

Polishing Steps	SiC paper	Lubricant	Polishing time (s)	Force (daN)	Rotation speed of the polishing disc (rpm)
1	P240	Ethanol ^(*)	30	0.25	150
2	P600	Ethanol	180	0.25	150
3	P1200	Ethanol	270	0.25	150
4	P2400	Ethanol	360	0.25	150
5	P4000	Ethanol	450	0.25	150

^(*) Absolute ethanol was used as polishing lubricant to avoid sample hydration reactions.

Table 6

Phase name	Formula	ICSD codes	Ref.
Orthorhombic ye'elimite	orth- $C_4A_3\bar{S}$	80361	[34]
Krotite	CA	260	[41]
Grossite	CA ₂	34487	[42]
Lime	C	52783	[43]
Anhydrite	C \bar{S}	15876	[44]